Final Report

DOE/AL/94649--T2

"EFFECT OF PULSATION

ON

BLACK LIQUOR GASIFICATION"

B. T. Zinn, J. Jagoda, H. Jeong,
A. Kushari and L. J. Rosen

"Laboratory for Pulse Combustion Processing"

School of Aerospace Engineering
Georgia Institute of Technology
Atlanta, GA 30332-0150

submitted to the

US Department of Energy
Grant # DE-Fg04-93AL~~9469~~ 94649

R. Balthaeser and G. Varga, Monitors

December 1998

DISCLAIMER

DISCLAIMER

Portions of this document may be illegible in electronic image products. Images are produced from the best available original document.

INTRODUCTION

Pyrolysis for the treatment of organic wastes has been gaining increasing interest over recent years. One such application is the pyrolysis of black liquor, a byproduct of paper making. Currently the paper making industry relies on recovery boilers burning black liquor to raise steam. There is a desire to move away from recovery boilers which is the single most expensive installation in the mill and gasify the black liquor in a fluidized bed. The black liquor gas, which has high energy content, could then be used to raise steam. Gasification has other benefits, including the ability to use the black liquor gas to supply heat to the gasification reaction and the separation of the salts in the black liquor, which can be recovered and reused for paper making.

In this process, it is critical that the temperature remains in a small window above the gasification temperature (1,000 ^{o}K) but below the smelting temperature (1,350 ^{o}K) of the inorganic salts in the black liquor. This would prevent the melting of the inorganic components of the black liquor such as sodium carbonate (Na_2CO_3), sulfide (Na_2S), and sulfate (Na_2SO_4), and any potassium salts that may be present in the bed. The presence of smelt would significantly increase agglomeration within the bed, which would inhibit bed fluidization. In addition, molten inorganic salts are known to cause serious corrosion problems during traditional molten liquor recovery. A pulse combustor combined with a fluidized bed might be well suited to provide the heat to the gasification reaction. There is a high convective heat transfer rate from the combustion products to the tail pipe wall, which means more of the energy will be transferred from the hot exhaust products to the fluidized bed in a smaller facility. Similarly, a fluidized bed has high heat transfer rates within the bed itself, promoting temperature uniformity throughout. By combining a pulse combustor with a fluidized bed as a means of supplying energy to the gasification process, we take advantage of the high heat transfer rates associated with both.

Pyrolysis is an endothermic process. The heat of reaction is provided either by partial combustion of the waste or by heat transfer from an external combustion process. In one proposed system [1] black liquor is pyrolized in a fluidized bed to which heat is added through a series of pulse combustor tail pipes submerged in the bed material. This system appears promising because of the relatively high heat transfer in pulse combustors [2] and in fluidized beds. Other advantages of pulse combustors are discussed elsewhere [3]. The above-described process is, however, only economically viable if a part of the pyrolysis products can be used to fire the pulse combustors.

The overall goals of this study were to determine: (1) which is the limiting heat transfer rate in the process of transferring heat from the hot combustion products to the pipe, through the pipe, from the tail pipe to the bed and through the bed; i.e., whether increased heat transfer within the pulse combustor will significantly increase the overall heat transfer rate; (2) whether the heat transfer benefits of the pulse combustor can be utilized while maintaining the temperature in the bed within the narrow temperature range required by the process without generating hot spots in the bed; and (3) whether the fuel gas produced during the gasification process can be used to efficiently fire the pulse combustor.

PYROLYSIS PRODUCTS AS PULSE COMBUSTOR FUELS

The performance of pulse combustors has been shown to depend critically upon the chemical composition of the fuel [4,5]. Additional difficulties in the operation of pulse combustors with pyrolysis products may be caused by the low heat content of these fuels, typically 12 MJ/m^3

compared to 40 MJ/m^3 for natural gas. It was the goal of this part of the study to investigate the effect of low heat content and relatively high hydrogen content of this fuel on the performance of pulse combustors.

Background

When a pulsed combustor operates at its limit cycle the acoustic driving of the pulsations by the oscillatory combustion process exactly balances the acoustic losses due to flapper valves, acoustic radiation and viscous effects. According to Rayleigh's criterion driving occurs when the pressure and heat release fluctuations are in phase. Quantitatively this balance between driving and damping at the limit cycle can be expressed as:

$$\int_V \int_T P' Q' \, dt d\upsilon = \int L_I \, dt \tag{1}$$

where P' and Q' are the instantaneous pressure and heat release rates and L_I the instantaneous sum of all losses. V is the volume of the combustor and T is the period of oscillation. Alternatively equation (1) can be written as:

$$\mathbf{P.Q}.\cos(f) = L \tag{2}$$

where **P** and **Q** are the pressure and heat release amplitudes, ϕ is the phase angle between them, and L is the sum of all losses during the cycle. Thus if ϕ is less than 90°, the heat addition process will drive the pressure oscillations, otherwise it will damp. A less well known second part of Rayleigh's criterion states that the frequency of pulsations increases if the heat release oscillations lead those in pressure and vice versa [6].

Combustion processes are never spontaneous. Keller et al. [7] have identified three distinct processes in pulsed combustion, which contribute to the total ignition delay time: (1) $t_{species}$, the time required for air and fuel to mix, (2) t_{mixing}, the time required for the incoming reactants to mix with the ignition source in the form of "hot products" remaining from the previous cycle, and (3) $t_{kinetic}$, the post mixing chemical ignition time. The total ignition delay time, $t_{ignition}$ is then given by:

$$t_{ignition} = f(t_{species}, t_{mixing}, t_{kinetic}) \tag{3}$$

The processes inside the combustor are complex. It is, therefore, not possible to entirely decouple the above three "characteristic" times. But in general, an increase in any of these times will result in an increase in overall ignition delay times. Since the heat release generally leads the pressure fluctuations a longer ignition delay time, results in a smaller phase angle. Three physical factors affect the ignition delay time in a given combustor, the reactant flow rates which affect the mixing, while the temperature and fuel composition determine the chemical time.

Experimental Set-up

A Helmholtz type, non-premixed, valved pulsed combustor was chosen for this study since its operation has been extensively investigated at the Laboratory for Pulse Combustion Processing at Georgia Tech [8,9]. However, the reported results are applicable to many other types of pulse combustors whose operation is governed by similar physical principles.

The test combustor consists of a mixing chamber, a combustion chamber, a tail pipe, a decoupler and a vent pipe, see Fig. 1. This figure also shows a cut-away view of the valve assembly and mixing chamber as an insert. Fuel and air enter sequentially at about 200 mm of water column and atmospheric pressure, respectively, through a pair of flapper valves radially into the combustor. Ignition is achieved by activating the spark plug while sequentially introducing air and fuel. The ensuing combustion and expansion processes increase the pressure inside the combustor, which closes the flapper valves, and expels hot combustion products through the tailpipe. Once the combustion process nears completion, the chamber pressure starts to decrease. When the chamber pressure drops below the fuel line pressure the fuel valve re-opens allowing fresh charges of fuel to enter the combustor. These mix with the air left from the previous cycle and are re-ignited by remaining pockets of burning gas, without the use of the spark plug. A little later during the cycle the combustor pressure drops below atmospheric and the air valve re-opens to admit a fresh charge of air. The rate of combustion now increases dramatically causing the pressure in the combustor to rise and to close the valves. This results in a periodic process that can continue indefinitely without the use of a spark plug. The fuel air ratio is varied by adjusting the air flapper valve while the fuel valve remains fixed.

The effect of heat content and composition of the fuel upon pulse combustor performance was quantified by determining acoustic pressures and heat release rates in the pulse combustor. The amplitudes and frequencies of the pulsations were measured using a water-cooled piezoelectric transducer mounted on the wall of the combustion chamber. Global reaction, and, therefore, heat release rates were obtained by measuring C-C radiation through a quartz window in the upstream end of the pulse combustor using a photomultiplier fitted with the appropriate optical narrow band pass filter. Heat release and acoustic pressure signals were acquired using a computer based data acquisition system running Labview. Fast Fourier Transforms (FFT) were performed on the raw data to obtain auto and cross spectra and, therefore, the phase angle between the pressure and heat release signals. Driving, as defined below, was calculated by integrating the product of the instantaneous pressure and heat release over one cycle using Simpson's rule [10]. Air and different fuel mixtures were measured upstream of the respective valves using calibrated flow meters, which were separated from the pulse combustor by decouplers.

Results and Discussion

Three series of tests were carried out in order to be able to separate the effects of low heat content from those of the chemical make up of the fuel:

(1) Burning methane diluted with carbon dioxide and helium to vary the heat content, keeping methane flow rate and fuel density constant.
(2) Burning methane-hydrogen mixtures diluted with carbon dioxide and helium to vary the heat content, keeping methane and hydrogen flow rates and fuel density constant.
(3) Burning various mixtures of methane and hydrogen diluted with carbon dioxide and helium, keeping power, fuel heat content, total fuel flow rate and fuel density constant.

Effect of Fuel Heat Content on Combustor Performance:

The effects of heat content in the fuel upon the operation of the pulse combustor were studied. Two series of tests were carried out, one with a constant flow rate of methane of $2.35*10^{-4}$ m^3/s, the other with constant flow rates of methane at $1.9*10^{-4}$ m^3/s and hydrogen at $1.48*10^{-4}$ m^3/s. This corresponds to a total power input of 8.793 kW for both fuels. In the case of

the methane-hydrogen mixture 80% of the energy available in the fuel is supplied by the former. In both cases various amounts of carbon dioxide and helium were added to the combustibles to reduce the heat content of the fuel. However, the proportions of diluents were carefully chosen to maintain flows of constant density, 0.6 kg/m^3 for pure methane and 0.45 kg/m^3 for the methane-hydrogen mixture. Air flow rates were also kept constant at $6.84*10^{-3}$ m^3/s for the former and $5.5*10^{-3}$ m^3/s for the latter. This means that the fuel air ratios were maintained constant, although the fuel flow rates had to change when the heat contents of each of the fuels were varied. The heat content of the mixtures was varied from just below that of pure methane (40 MJ/m^3) to that typical for black liquor pyrolysis products (12 MJ/m^3).

Figures 2a-d show the variations of amplitude of the heat release and pressure fluctuations, their frequency and the phase angle between them for methane and methane-hydrogen fuels. The pulse combustor operates well for both fuel types down to heat contents of 10-12 MJ/m^3. Operation with fuels of lower heat content requires a high fuel supply pressure, which no longer allows the flapper valve to close. As a result the fuel enters the combustor throughout the cycle and the pulsations become very weak. The highest achievable heat content is higher for methane than for the methane-hydrogen mixture since hydrogen has a lower calorific value than methane.

There are some clear differences in the behavior of the pulse combustor when fired with the two fuels. For methane fuels the sound pressure level and frequency of operation show very slight increases with heat content, especially for lower calorie fuels. However, if 20% (by heating value) of the methane is replaced by an equivalent amount of hydrogen the sound pressure level decreases with increasing heat content while the pulse frequency first increases and then levels off, see Fig. 2a and b.

The explanation for this behavior can be found in the trends of phase angle and heat release fluctuations as a function of heat content in the fuel as shown in Figs. 2c and d. For a given phase angle the heat release amplitudes are directly proportional to the acoustic driving, i.e., the pressure amplitudes increase with increasing heat release fluctuations. On the other hand, for a given heat release amplitude, an increase in phase angle decreases the acoustic driving and thus the pressure amplitudes. The phase angle and the heat release fluctuations increase with heat content for both types of fuel. Thus there are competing effects when the heat content in the fuel is increased. The amplitudes of the heat release fluctuations increase at approximately the same rate for both types of fuels. However, the phase angle between heat release and pressure fluctuations at a given heat content are significantly larger for the hydrogen containing fuels than for those with only methane. As a result, the driving force and, therefore, the pulsation amplitudes are smaller for hydrogen containing fuels than for methane fuels with equal heat content.

According to Rayleigh's criterion, the larger phase angle for hydrogen containing fuels is also responsible for the higher frequencies observed for these fuels. However, changes in temperature in the pulse combustor caused by the variation in air flow rate affect the speed of sound and can therefore, also lead to slight changes in the resonance frequency.

It is clear from the above discussion that the relative timing of the heat release with respect to the pressure cycle is critical for the operation of the pulse combustor. Since the oscillations in heat release lead those in pressure, a larger phase angle in Fig. 2c means an earlier heat release during the cycle. Thus, combustion occurs later in the cycle when the heat content in the fuel is reduced for both types of fuel. This may be due to less efficient mixing between the reactants and with the ignition sources caused by the presence of large quantities of diluents or to longer post mixing chemical ignition delay times caused by lower temperatures in the combustor.

Furthermore, the fuel containing hydrogen ignites earlier during the cycle than the methane fuel because of the difference in combustion chemistry between methane and hydrogen or the increased mixing in the case of hydrogen fuels since the lower heat content of hydrogen requires higher fuel flow rates for a given heat requirement. This, in turn, may lead to higher levels of turbulence, and thus more efficient mixing.

Separating the Chemistry from the Fluid Mechanics

In order to fully understand the above results it must be possible to separate the effects of fluid mechanics from those of the chemistry. During previous investigations [4] of the effect of hydrogen in the fuel on the operation of pulse combustors, hydrogen was either added to or replaced parts of the methane flow. During all these tests the flow rates as well as the composition of the fuel was changed. In the tests described below judicious choices of diluents assured that fluid flow conditions remained constant even though the fuel composition was varied.

Different proportions of Methane and Hydrogen were mixed with carbon dioxide and helium to produce fuels of constant heat input per unit time (14.7 kW) and per unit volume of fuel (17.93 MJ/m^3), constant volume flow rate ($8.17*10^{-4}$ m^3/s, constant density (0.45 kg/m^3) and therefore, constant mass flow rate. In addition, the heat capacity of the fuel changed by less than 10%. The diffusivity of the fuel mixtures could not be kept constant. However, in the highly turbulent environment in the pulse combustor [11], turbulent mixing rather than diffusion dominates the transport processes. As a result the fluid mechanically controlled mixing remains essentially constant when the fuel composition is changed as long as the air flow rate remains constant. Any observed changes must, therefore, be entirely due to differences in chemical delay times for the different fuels.

Figure 3 shows the dependence of sound pressure level and frequency of pulsations upon hydrogen content in the fuel for an air flow rate of $6.3*10^{-3}$ m^3/s, similar to the air flow rates used in the above tests. The percentages of hydrogen in these figures refer to the fraction of total heat content of the fuel derived from hydrogen for the particular mixture. Clearly the sound pressure level decreases while the frequency of pulsations increases as the hydrogen content in the fuel increases. The reason for this can be seen in Fig. 4. The phase angle by which the heat release leads pressure fluctuations increases with hydrogen content in the fuel, which causes the frequency of pulsation to rise. Also shown in Fig. 4 is the acoustic driving integrated over one cycle for various fuel compositions. It significantly decreases with increasing hydrogen content, primarily due to the increase in phase angle shown in Fig. 4. This results in the significant decrease in sound amplitude presented in Fig. 3. Comparing these results with those in Figs 2 a-d strongly suggests that the reduction in sound pressure level and frequency of pulsations observed in Fig. 2 are, indeed, primarily due to changes in combustion chemistry once hydrogen is introduced.

One additional observation of interest should be mentioned at this time. Table I shows the range of equivalence ratios over which pulsating operation could be sustained. Clearly, the addition of hydrogen extends the rich limit of operation of the pulse combustor significantly. It has previously been shown [11] that fuel, which is supplied through a pressurized line, enters the pulse combustor much earlier in the cycle than fresh air. Furthermore, it was determined that the duration of the cycle is insufficient to permit complete combustion unless the fuel can burn immediately after entry with air left over from the previous cycle. Thus, the combustor reaches a rich limit of operation near stoichiometric fuel and air flow rates when little air remains for the next cycle. During previous tests this limit could only be extended if the duration of the cycle was extended by changing combustor geometry or by injecting the reactants earlier in the cycle by

increasing their supply pressure. In the tests being reported here this limit could be significantly extended by accelerating the combustion process through the addition of hydrogen to methane.

HEAT TRANSFER IN P/C TAILPIPES SUBMERGED IN A FLUIDIZED BED

The objective of this part of the research program was to develop a better understanding of the heat transfer mechanism from the oscillating flow in a pulse combustor tail pipe to a fluidized bed. Specifically it was to be determined: (1) which is the limiting heat transfer rate in the process of transferring heat from the hot combustion products to the tail pipe, through the pipe, from the tail pipe to the fluidized bed and then through the bed itself (that is, whether increased heat transfer within the pulse combustor will significantly increase the overall heat transfer rate) and (2) whether the temperature distribution in the bed can be maintained within a narrow temperature range without generating hot spots in the bed even if the heat transfer from the tail pipe is significantly increased. This understanding is necessary to design a system in which pulse combustion provides the energy required for the endothermic gasification of black liquor and other organic wastes in a fluidized bed.

Background

Heat Transfer for Pulsating Flow

Recently, there have been a number of active research programs on pulse combustion because its application in energy intensive processes may lead to fuel savings, reduced pollutant formation, high combustion intensity, increased convective heat transfer rates and lower operating and equipment costs [3]. Pulsating combustors are characterized by the presence of fluctuating pressure and velocity components. The presence of acoustic oscillations is apparently also responsible for increased gas phase mixing. It is also generally accepted that if the pulsations are strong enough that the flow reverses direction, the pulsations result in considerable enhancement of convective heat transfer rates from the flow to the surrounding boundaries. These high heat transfer rates can be utilized to create low cost, compact heat exchangers, while in other situations the effect is undesirable and can result, for example, in the melting of the walls of liquid propellant rocket motors after the onset of a combustion instability. It is, therefore, important to understand how oscillating flows enhance convective heat transfer and how the enhancement is related to flow conditions in order to utilize high heat transfer effect or prevent it causing undesirable effects.

Hanby [12] investigated convective heat transfer in a gas-fired pulsating combustor that resonated as a quarter-wavelength pipe at a frequency of 100 Hz. He showed that the heat transfer coefficient depends upon the local flow condition and that it reaches a maximum at the location of maximum acoustic velocity amplitude near the exit of the combustor. His maximum heat transfer rate enhancement is of the order of 2.4 when the ratio of the velocity oscillation amplitude to mean velocity is 5. Alhaddad and Coulman [13] also performed similar experiments. Their frequency ranged from 45 to 60 Hz for flows with mean Reynolds number between 2,432 to 7,892. They show that heat transfer rate enhancement is of the order of 0.7, that is, pulsation reduced the heat transfer rate by 30%. Liao and Wang [14] investigated heat transfer from pulsating turbulent water pipe flow at frequencies between 0.07 and 0.4 Hz for flows with mean Reynolds numbers in the range from 3,400 to 27,000. They also showed a decrease in heat transfer coefficient when the ratio of the velocity oscillation amplitude to mean velocity is

between 0.3 and 2. Keil and Baird [15] investigated the effect of pulsation in water flow on the overall heat transfer coefficient of a shell-and-tube heat exchanger with steam in the shell. Their frequency ranged from 0.4 to 1.1 Hz. Their maximum heat transfer rate enhancement is of the order of 2 when the ratio of the velocity oscillation amplitude to mean velocity is 8. Galitseyskiy and Ryzhov [16] investigated heat transfer in turbulent gas flow in channels at frequencies ranging from 90 to 1,000 Hz for flows with mean Reynolds number between 10,000 and 200,000. Their maximum heat transfer rate enhancement is of the order of 6. Dec and Keller [17] investigated heat transfer in oscillating flows of a Helmholtz type pulse combustor tail pipe at frequencies between 70 and 100 Hz and mean Reynolds numbers between 3,100 and 4,700. Their maximum heat transfer rate enhancement is of the order of 2.5 when the ratio of the velocity oscillation amplitude to mean velocity is 5.07. Their investigation included the velocity measurement and spatial temperature measurement using two-line atomic fluorescence (TLAF). Jackson and Purdy [18] investigated heat transfer in resonant pulsating flows for frequencies between 170 and 360 Hz and mean Reynolds number ranging from 2,050 to 11,600. In their experiment the sound field is produced by two conventional drivers and a conical horn that was mounted at the exit of the test section. They showed that the local heat transfer coefficient is maximum at the velocity antinode or pressure node of the standing wave. Their overall increase of heat transfer rate is approximately 20 % for the 2050 Reynolds, 221 Hz frequency, and 162.5 dB sound pressure level condition.

The results of this previous research show that the velocity oscillation with amplitudes less than the mean decrease the heat transfer rate, but velocity oscillations with amplitudes greater than the mean velocity increase the heat transfer rate significantly. These heat transfer rates have been measured several methods such as using a suction pyrometer probe [12], measuring the condensation collected [15,18], and two wall-thermocouple [14,17].

Many studies in the literature have been carried out at frequencies lower than 100 Hz, typical of pulse combustors [12,13,14,15,17]. In addition, there were a few studies in which axially resolved heat transfer coefficients were obtained [17,18]. Dec and Keller [17] measured the local heat transfer coefficients for just 4 axial positions. Jackson and Purdy [18] investigated the local heat transfer coefficients for a constant temperature horizontal tube. However in a practical reactor the temperature decreases in the axial direction as heat is transferred out of the flow. Therefore, one of the goals of this research is to investigate the axially resolved local heat transfer coefficient for a horizontal tube with axial temperature gradient. An enthalpy difference method is used to obtain the local heat transfer rate that permits us to obtain fine axial resolution.

Heat Transfer in Fluidized Beds

A number of fundamental studies dealing with heat transfer from the surface of an immersed object (rod or cylinder) to a fluidized bed have been reported in the literature. Gel'prein, Ainshtein, and Zaikovskii [19] performed an experimental investigation of the variation of local heat transfer coefficient in the cross section of a horizontal tube in a small particle fluidized bed by measuring local temperature differences and local heat flux powers. Berg and Baskakov [20] investigated the local heat transfer between a fixed horizontal cylinder and a fluidized bed. They showed the distribution of the relative heat transfer coefficient (ratio local to average heat transfer coefficient) around a horizontal cylinder surface. Both Gel'prein [19] and Berg [20] obtained, essentially, the same results. They found that the local relative heat transfers coefficients were maximum at the side and minimum at the bottom and top of the immersed tube. It appears that the flow across the pipe generates regions of low velocity near the stagnation

points, which reduce the local heat transfer coefficient. These regions are called a gas "bag' below and a "cap" above the tube.

Newby and Keairns [21] investigated fluidized bed heat transfer between parallel horizontal tube-bundles. In their results, tube to bed heat transfer coefficients for centrally located tubes were increased by the presence of compact tube bundles. Grewal and Saxena [22] measured the heat transfer coefficient between an electrically heated single horizontal tube and air-solid fluidized beds, of several different materials. They investigated the effect of size, shape, and density of the particle, air mass fluidizing velocity, tube size, tube material, and bed depth on heat transfer rate. The heat transfer coefficient decreased with increasing particle diameter. This is predominantly due to an increase in the average gas conduction paths between the heat transfer tube and the first row of particles and between particles as their size increase. Clement [23] investigated the heat transfer coefficient in a horizontal tube immersed in a fluidized bed of large particles. He investigated some parameters such as the effective thermal conductivity, the gas film thickness, the emulsion contact time, and bubble voidage for the accurate prediction of the overall heat transfer coefficient. Suarez [24] also investigated heat transfer coefficient from a horizontal tube immersed in a mixed particle size, gas-fluidized beds. He conducted flow visualization for a horizontal cylinder immersed in a fluidized bed of spherical glass particle. All this previous research were conducted for constant surface temperature maintained by an electrical heater in small (less than 300 μ) or large (greater than 800 μ) particle fluidized beds.

In these previous studies heat transfer coefficients between constant temperature tail pipes and the fluidized bed were measured and calculated. One of the goals of this research is to investigate the local heat transfer coefficient from a tail pipe surface, whose temperature is decreasing along the pipe, to a fluidized bed. This is a more realistic model of the situation in a fluidized bed reactor with immersed heat pipes.

Methodology

In previous studies local heat transfer coefficients were measured using a suction pyrometer, two wall thermocouple, and measuring collected condensates. Here local heat transfer coefficients were calculated from measured center line temperatures. This technique of determining heat transfer from enthalpy difference calculated from the measured center line temperature has the advantage that it permits fine axial resolution. Selected values have been checked against direct measurements obtained using the heat flux sensors. Heat transfer coefficients in the fluidized bed itself were calculated by measuring inner wall, outer wall, and bed temperatures. These experiments were conducted under conditions of natural and forced convection, i.e., outside and inside a fluidized bed. Heat transfer rates in the fluidized bed away from the submerged tailpipe was measured using thermocouples placed in the bed radially outward from the pipe.

The experimental values for the heat transfer coefficients in the tail pipe and fluidized bed itself have been compared with theoretical results obtained as part of this study. Quasi-steady theory was adapted for calculating local heat transfer coefficients inside the tail pipe. An empirical correlation was used to calculate the heat transfer coefficient from the outer wall of the pipe for natural convection. Modified packet renewal theory was used for calculating the heat transfer coefficient from the outer wall of the pipe to the fluidized bed itself. A center line temperature was calculated using the isothermal boundary condition. Calculated centerline temperatures were then compared with measured values.

Theoretical Studies

Heat transfer coefficients from the hot gas to the inner tail pipe wall and from the outer wall to the surrounding material were calculated for both natural convection and forced convection in a fluidized bed. In addition, the center line temperature and the outer wall temperature were calculated using theoretically determined heat transfer coefficients. Theoretically and experimentally obtained values are compared whenever possible.

Calculation of heat transfer coefficient from the hot gas to the inner wall of the tail pipe

The convective heat transfer coefficient for turbulent flows in pipes has been correlated with Prandtl and Reynolds numbers by Dittus-Boelter [25]

$$Nu_D = 0.023\,\mathrm{Pr}^n\,\mathrm{Re}^{0.8} \tag{4}$$

which was developed for $0.7 \le \mathrm{Pr} \le 1200$, $2500 \le \mathrm{Re}_D \le 1.24 \times 10^5$, and L/D >60.
Equation (4) is equivalent to

$$\frac{hD}{K} = 0.023\left(\frac{C_p\mu}{K}\right)^n\left(\frac{VD}{\nu}\right)^{0.8} \tag{5}$$

The Prandtl number exponent, n=0.4 when the fluid is being heated ($T_o > T_m$), and n=0.3 when the fluid is being cooled ($T_0 < T_m$). All the physical properties needed to calculate Nu_D, Re_D, and Pr are evaluated at the bulk (mean) temperature T_m. The maximum deviation between experimental data and values predicted using equation (4) for steady flow is of the order of 40 percent [26].

Most attempts to model the heat transfer in oscillating flows resort to using steady or quasi-steady assumptions [17]. That means that, at any point in the cycle the flow is assumed to behave as if it were steady at the instantaneous velocity. This assumption is valid only for flows with low frequency oscillations, since it requires that the flow become steady within a time much less than the duration of a cycle. The first known use of this approach was by Martinelli in 1943 [27]. Since then, it has been used by several other researchers [12,14,15].

In this model the instantaneous velocity of the gas can be represented as a superposition of an acoustic (or sinusoidal) velocity on a steady flow :

$$V = V_m(1 + B\cos wt) \tag{6}$$

By substituting V into the correlation given by equation (5), one obtains for the instantaneous heat transfer coefficient

$$h = 0.023\frac{K}{D}\left(\frac{C_p\mu}{K}\right)^{0.3}\left(\frac{V_m D}{\nu}\right)^{0.8}\{1 + B\cos\omega t\}^{0.8} \tag{7}$$

The mean value over one cycle is here given by

$$\bar{h} = \frac{1}{2\pi}\int_0^{2\pi} h\,d\omega t \tag{8}$$

$$h_i = \bar{h} = h_{ave} = 0.023\frac{K}{2\pi D}\left(\frac{C_p\mu}{K}\right)^{0.3}\left(\frac{V_m D}{\nu}\right)^{0.8}\int_0^{2\pi}\{1+B\cos\omega t\}^{0.8}\,d\omega t \qquad (9)$$

The local air properties can be obtained from the measured center line temperature. The amplitude of the velocity oscillation can be obtained using acoustic velocity and pressure relationship from 1-D plane acoustic wave momentum equation. The mean velocity of flow can be also obtained using conservation of mass at each location. Consequently, the ratio of the amplitude of the velocity oscillation to the mean velocity B can be obtained at each local position. Then the local heat transfer in a pulsating flow can be predicted using equation (9).

Calculation of the heat transfer coefficient from an outer wall for natural convection

In this section, the external heat transfer coefficient for natural convection is calculated. Churchill and Chu [28] have recommended Nusselt number correlation for the natural convective flow around a cylinder positioned horizontally in an isothermal fluid for a wide Rayleigh number range. Their correlation equation is used to calculate the external heat transfer coefficient h_e.

$$Nu_D = \frac{h_e D_e}{K_{ext}} = \{0.6 + \frac{0.387 Ra_D^{\frac{1}{6}}}{[1+(0.559/\Pr)^{\frac{9}{16}}]^{\frac{8}{27}}}\}^2 \quad 10^{-5} < Ra_D < 10^{12} \qquad (10)$$

where the Rayleigh number is the product of Grashof and Prandtl numbers.

$$Ra_D = \frac{g\beta(T_o - T_\infty)D_e^3}{\nu\alpha} \qquad (11)$$

Calculation of the heat transfer coefficient from an outer wall for forced convection in a fluidized bed

Several theories have been proposed by investigators in an attempt to explain the high rate of heat transfer rates observed in fluidized beds. Many factors influence the rate of heat transfer. The heat is transferred from the wall surface to the fluidized bed by three mechanisms [29]:

(1) By particles being brought into contact with the surface, residing there and absorbing heat and then being replaced by fresh particles. This component, h_{pc}, is termed the "Particle convective" heat transfer coefficient.

(2) By convective heat transfer between the interphase gas and surface. This component, h_{gc}, is termed the "Gas convective" heat transfer coefficient.

(3) By radiation, this component, h_{rad}, is termed the "Radiative" heat transfer coefficient. This component, however, is negligible when the bed temperature is less than 1,000 $^\circ F$ (600 $^\circ C$) [21].

The particle convective heat transfer coefficient is dominant for fine particles, while the gas convective component become increasingly important as the particle size is increased [30]. The radiative component is not considered in this research because the operating temperature is kept below 1,000 $^\circ F$.

The particle convective heat transfer coefficient

Several physical models for the particle convective heat transfer coefficient are suggested in the literature. The Packet Renewal Theory is based on unsteady heat transfer between a heat transfer surface and a packet of particles (i.e. emulsion), which is brought into contact with the surface. The packet resides on the surface for a short time, and the residence time is terminated when the packet is swept away by rising bubbles within the bed. This model was first proposed by Mickley and Fairbanks [31].

Xavier and Davidson suggested a more sophisticated modified packet renewal theory [32]. It recognizes that the packets of particles are separated by layers of gas from the immersed pipe. This results in a two step heat transfer process :

(1) Heat transfer by unsteady state conduction through a gas layer adjacent to the surface.

(2) Heat transfer by unsteady state diffusion from the gas layer to the particulate phase.

Experimentally, it has been shown that the heat transfer coefficient between a fluidized bed and an immersed surface decreases as the particle diameter increases. Therefore, an explicit dependence of heat transfer coefficient on the particle diameter should exist, which can be obtained by considering a gas film of average thickness, δ, between the surface and particulate phase. This gas film offers a resistance to heat flow. Its thickness may be related to the particle diameter in such a way that as the particle diameter increases the gas film thickness increases [33].

Consider an elemental volume of an emulsion packet of unit height and width and of length, $\delta\eta$, in the direction of heat flow. δ is normal to the pipe surface, see Fig. 5.

The following assumptions are made [32]:

(1) Unsteady state heat conduction through a gas film of thickness, δ, around the pipe.

(2) No variation in bed properties with angular position around the pipe.

(3) Unsteady state heat transfer from the pipe surface through the gas film to the packet of particles.

(4) The packet has a contact time, τ, after which it is replaced by the passage of a bubble.

(5) The particle packet has the properties of the bed at minimum fluidization.

(6) The temperature of the part of the packet far from the pipe surface remains unchanged at $T_{b\infty}$ during the residence time.

The differential form of the Fourier Law of heat conduction equation states that the heat flux in the direction of increasing η is :

$$q_\eta = -K\frac{\partial T}{\partial \eta} \tag{12}$$

The heat flux into the elemental volume in Fig. 5 is

$$dq_\eta = -K_{mf}\frac{\partial T}{\partial \eta} \quad \text{and} \tag{13}$$

$$dq_{\eta+d\eta} = dq_\eta + \frac{\partial}{\partial \eta}(dq_\eta)d\eta \tag{14}$$

The time rate of change of energy storage in the volume element is

$$\rho_{mf} C_{mf} \left(\frac{\partial T}{\partial t}\right) \delta\eta \tag{15}$$

The rate of energy generation in the volume element is zero. Performing an energy balance on the volume element results in the following equations:

$$dq_\eta = dq_\eta + \frac{\partial}{\partial \eta}(dq_\eta)\delta\eta + \rho_{mf} C_{mf} \left(\frac{\partial T}{\partial t}\right)\delta\eta \tag{16}$$

i.e. $$-\frac{\partial}{\partial \eta}(dq_\eta)\delta\eta = \rho_{mf} C_{mf} \left(\frac{\partial T}{\partial t}\right) \tag{17}$$

Substituting Fourier's Law of heat conduction

$$-\frac{\partial}{\partial \eta}\left(-K_{mf} \frac{\partial T}{\partial \eta}\right) = \rho_{mf} C_{mf} \left(\frac{\partial T}{\partial t}\right) \tag{18}$$

If the emulsion packet is assumed to be homogeneous and isotropic, equation (18) becomes

$$K_{mf} \frac{\partial^2 T}{\partial \eta^2} = \rho_{mf} C_{mf} \frac{\partial T}{\partial t} \tag{19}$$

or

$$\alpha_{mf} \frac{\partial^2 T}{\partial \eta^2} = \frac{\partial T}{\partial t} \tag{20}$$

If the excess temperature, U, at a specified η is defined as

$$U = T_w - T \tag{21}$$

then

$$\frac{\partial^2 U}{\partial \eta^2} = -\frac{\partial^2 T}{\partial \eta^2} \tag{22}$$

$$\frac{\partial U}{\partial t} = -\frac{\partial T}{\partial t} \tag{23}$$

Thus, the governing equation for this unsteady conduction through the gas film and emulsion is

$$\alpha_{mf} \frac{\partial^2 U}{\partial \eta^2} = \frac{\partial U}{\partial t} \tag{24}$$

The initial condition is a uniform temperature in the packet at time zero, i.e. the bed temperature at any specified η is the same as the bed temperature at $\eta=\infty$.
Therefore, at t=0,

$$U = T_w - T_\eta \tag{25}$$

and

$$U_\infty = T_w - T_{b\infty} \tag{26}$$

since

$$T_\eta = T_{b\infty} \quad \text{at } t=0 \tag{27}$$

then

$$U = U_\infty \text{ at } t=0 \tag{28}$$

The dependence of h_{pc} on particle diameter may be obtained by considering a contact residence at the surface, due to a gas film of conductivity K_g and average thickness δ; δ is proportional to particle diameter and the resulting heat transfer coefficient h_{film} is given by

$$h_{film} = \frac{K_g}{\delta} \tag{29}$$

Then, the boundary condition between the gas film and the surface of the packet at $\eta=0$ is

$$K_{mf}\frac{\partial T}{\partial \eta} = \frac{K_g}{\delta}(T_w - T_\eta) \quad \text{at } \eta=0 \tag{30}$$

or

$$K_{mf}\frac{\partial U}{\partial \eta} = \frac{K_g}{\delta}U \qquad \text{at } \eta=0 \tag{31}$$

If λ is defined as

$$\lambda = \frac{K_g}{\delta K_{mf}} \tag{32}$$

then, the boundary condition becomes

$$\frac{\partial U}{\partial \eta} = \lambda U \qquad \text{at } \eta=0 \tag{33}$$

Thus, the differential equation to be solved is

$$\alpha_{mf} \frac{\partial^2 U}{\partial \eta^2} = \frac{\partial U}{\partial t} \tag{34}$$

with initial condition

$$U = U_\infty \qquad \text{at } t=0 \tag{35}$$

and boundary condition

$$\frac{\partial U}{\partial \eta} = \lambda U \quad \text{at } \eta=0 \tag{36}$$

and

$$U = U_\infty \qquad \text{at } \eta \to \infty \tag{37}$$

The solution of above governing equation with given initial and boundary condition is given by Carslaw and Jager [34]:

$$\frac{U}{U_\infty} = \text{erf}\frac{\eta}{2\sqrt{\alpha_{mf} t}} + \exp[\lambda\eta + \lambda^2 \alpha_{mf} t] \bullet \text{erfc}[\frac{\eta}{2\sqrt{\alpha_{mf} t}} + \lambda\sqrt{\alpha_{mf} t}] \tag{38}$$

The instantaneous heat transfer coefficient is determined in the following way: the heat flux q is given by

$$q = h_i (T_w - T_{b\infty}) \tag{39}$$

and across the gas film as

$$q = \frac{K_g}{\delta}(T_w - T_0) \tag{40}$$

Equating the two equations for heat flux results in

$$\frac{h_i \delta}{K_g} = \frac{(T_w - T_0)}{(T_w - T_{b\infty})} \tag{41}$$

Applying the boundary condition (35)

$$\lambda(T_w - T_0) = \frac{\partial T_h}{\partial \eta}\Big|_{\eta=0} \tag{42}$$

we get

$$\frac{(T_w - T_0)}{(T_w - T_{b\infty})} = \exp[\lambda^2 \alpha_{mf} t] \bullet \operatorname{erfc}[\lambda\sqrt{\alpha_{mf} t}] \tag{43}$$

The instantaneous heat transfer coefficient is

$$h_i = \frac{K_g}{\delta} \exp[\lambda^2 \alpha_{mf} t] \bullet \operatorname{erfc}[\lambda\sqrt{\alpha_{mf} t}] \tag{44}$$

The time average heat transfer coefficient is

$$h_{ave} = \frac{\int_0^\tau h_i \, dt}{\int_0^\tau dt} \tag{45}$$

Applying this to equation (41) results in;

$$h_{ave} = \frac{\delta}{K_g} \frac{K_{mf} \rho_{mf} C_{mf}}{\tau} \{\operatorname{erfc}[\frac{K_g}{\delta}\sqrt{\frac{\tau}{K_{mf} \rho_{mf} C_{mf}}}] \bullet \exp[(\frac{K_g}{\delta})^2 \frac{\tau}{K_{mf} \rho_{mf} C_{mf}}] - 1\} + 2\sqrt{\frac{K_{mf} \rho_{mf} C_{mf}}{\pi\tau}} \tag{46}$$

If the gas film thickness δ is very thin, the above equation tends to the packet renewal theory. An average heat transfer coefficient can be calculated using equation (46). This average heat transfer coefficient, however, is not the particle convective heat transfer coefficient since it does not take into account that bubbles exist in the fluidized bed.

If the bubble phase in a fluidized bed occupies the volume fraction ε_B, then the average particle convective heat transfer coefficient is

$$h_{pc} = (1 - \varepsilon_B) h_{ave} \tag{47}$$

The gas flow above that of minimum fluidization velocity goes into the bubble phase, therefore

$$V_A \varepsilon_B = V - V_{mf} \tag{48}$$

where V_A is the absolute velocity of rising swarms of bubbles and is given by Kunii and Levenspiel [33].

$$V_A = V - V_{mf} + V_B \tag{49}$$

Combining both equations

$$\varepsilon_B = \frac{V - V_{mf}}{V - V_{mf} + V_B} \tag{50}$$

hence

$$1 - \varepsilon_B = \frac{V_B}{V_A} \tag{51}$$

For a single rising bubble, the bubble velocity is given by Davidson [29]

$$V_B = 0.711\sqrt{gD_B} \tag{52}$$

where $\mathbf{D_B}$ is the diameter of a sphere having the same volume as the bubble.

The bubble diameter can be evaluated by Mori and Wen [35].

$$D_B = D_{BM} - (D_{BM} - D_{B0})\exp[\frac{-0.3H}{d_c}] \tag{53}$$

where

$D_{BM} = 0.652[A_t(V - V_{mf})]^{\frac{2}{5}}$ is the maximum bubble diameter

$D_{B0} = 0.00376(V - V_{mf})^2$ is the initial bubble diameter

d_c is the bed diameter

H is the height above the distributor plate

A_t is the cross-sectional area of the fluidized bed

Finally, the local particle convective heat transfer coefficient can be written as

$$h_{pc} = \frac{V_B}{V_A}\frac{\delta}{K_g}A_1\{\text{erfc}[\frac{K_g}{\delta}\sqrt{\frac{1}{A_1}}] \bullet \exp[(\frac{K_g}{\delta})^2\frac{1}{A_1}] - 1\} + 2\frac{V_B}{V_A}\sqrt{\frac{A_1}{\pi}} \tag{54}$$

where $A_1 = \dfrac{K_{mf}\rho_{mf}C_{mf}}{\tau}$

The local particle convective heat transfer coefficient can be obtained using equation (54) if the thermal conductivity of the emulsion phase $\mathbf{K_{mf}}$, the gas film thickness δ, and the emulsion packet residence time τ are known. Thus, the next section will deal with determining these properties.

The thermal conductivity of the emulsion phase:

The properties of each packet are assumed to be equal to those of the particles in the bed at minimum fluidization. These properties can be deduced from those of the packed bed.

Swift assumed that all heat transferred was normal to a submerged surface and that the particles were packed in an orthorhombic way. As results K_e^0 was correlated as [36]

$$K_e^0 = 0.9065 \frac{2}{\frac{1}{K_s} - \frac{1}{K_g}} \left[\frac{K_s}{K_s - K_g}\left(\ln \frac{K_s}{K_s} - 1\right)\right] + 0.0935 K_g \tag{55}$$

Krupizcka conducted an extensive study on the thermal conductivity of granular materials and proposed the following general correlation [37].

$$\frac{K_e^0}{K_g} = \left(\frac{K_s}{K_g}\right)^{A + B \log \frac{K_s}{K_g}} \tag{56}$$

For the case of spherical particles, the constants are: A=0.583 and B=-0.063

It is reasonable to expect that the thermal conductivity of a bed at minimum fluidization conditions, K_{mf}, may be approximated by the effective thermal conductivity of a packed bed when the velocity of the gas flowing through it is equal to V_{mf}. Thus the thermal conductivity of the emulsion phase can be calculated from

$$K_{mf} = K_e^0 + 0.1 \rho_g C_g d_p V_{mf} \tag{57}$$

The gas film thickness

The mean value of the gas film thickness on a vertical surface is given by Zabrodsky [38].

$$\delta = \frac{d_p}{6} \tag{58}$$

Botterill and Williams [39] and Botterill and Desai [40] used in their calculation a gas film thickness of

$$\delta = \frac{d_p}{10} \tag{59}$$

The gas film thickness on a vertical surface (minimum value) lies in the range $\frac{d_p}{6}$ to $\frac{d_p}{10}$. The gas film thickness of the thickness on a horizontal surface (maximum value) is about twice that on a vertical surface. Therefore, the variation of the gas film thickness around the pipe surface can be approximated by following equation.

$$\delta = \delta_{\min}(1 + |\mathrm{Cos}\theta|) \tag{60}$$

where θ is measured from the stagnation point on the pipe surface and δ is the gas film thickness at the lateral sides of the pipe (that is, $\theta=90^0$ or 270^0).

The emulsion packet residence time

One of the main advantage of the packet renewal theory of heat transfer in fluidized beds is that the mathematical formulation is precise. However, the major drawback to the application of the model is the lack of information regarding the emulsion and void phase contact time on the surface of an immersed object in a fluidized bed.

Ozkaynak and Chen [41] investigated the residence time characteristics for both the emulsion and void phase in a fluidized bed by using a capacitance probe on the side of a vertically immersed tube. Changes in phase contact (void or emulsion) at the test tube surface were signaled by changes in the capacitance of the probe circuit. Typical output signals showed that the measured capacitance fluctuated between minimum and maximum values. The minimum capacitance approached that for air, while maximum capacitance approached that for a packed medium. Thus when the emulsion phase contacted the test tube surface, the sensing probe measured a capacitance approaching that of a packed bed. When a bubble void contacted the test tube surface, the signal jumped to a capacitance value close to that for air alone.

Residence time for the emulsion phase, τ_e was defined as the duration of contact by emulsion phase between successive bubble voids. Residence time of bubble void phase was defined as the duration of contact with the void between successive emulsion occupancies.

Ozkaynak and Chen [41] showed that the τ_e is very long at air flow rates close to minimum fluidization and decreases rapidly with increasing flow rate. Furthermore, increasing particle diameter increases the average residence time of the emulsion phase for a given air flow rate $(V\text{-}V_{mf})$.

The emulsion residence time, τ, void residence time, τ_b, frequency of replacement n, and the fraction of the total time that the surface is covered by voids, f_o, are related by the following

$$1-f_0=\frac{\tau_b}{\tau+\tau_b} \tag{61}$$

$$1-f_0=n_e\tau \tag{62}$$

$$f_0=n\tau_b \tag{63}$$

The emulsion residence time can be calculated by the following method.

$$\tau=\frac{1}{n}-\tau_b \tag{64}$$

Thus, if the bubble (void) phase contact time τ_b, and replacement frequency, n, can be determined, the emulsion phase residence time τ_e on a surface can be calculated.

The bubble phase residence time on a surface can be calculated from

$$\tau_b = \frac{D_B}{V_B} \tag{65}$$

where $_B$ is the bubble velocity

Cranfield and Geldart [42] measured the bubble concentration and bubble frequency at bed depth up to 30 cm in a large particle fluidized bed. They concluded that the bubble frequency was relatively insensitive to gas velocities and showed a steady decrease with the bed height. They also assumed that the bubble frequency remains unchanged when the gas flow rate is changed. Their data were correlated as

$$n = 16.7H^{-0.72} \tag{66}$$

where H is the bed height

The emulsion packet residence time τ can then be obtained using equation (61).

The gas convective heat transfer coefficient

The gas convective part of the overall heat transfer coefficient is usually small but under some conditions it is important [29]. These are:

(1) Higher operating pressure
(2) High gas velocity
(3) Large particle diameter
(4) Gas velocity near the minimum fluidization

Until recently, not much attention has been paid to the gas convective heat transfer component in fluidized bed, since fluidization technique have been applied most extensively in fine particle system where the fluidization velocity is small. Several approach have been adopted in an attempt to estimate the gas convective heat transfer coefficient.

Many investigators have assumed packed bed condition in their attempt to determine the gas convective heat transfer rate. Gabor [43] formulated a simple model for estimating the gas convective component.

Baskakov and Surprum [44] performed some experiments on mass transfer from Naphthalene surface to packed and fluidized beds, and by means of the analogy between mass and heat transfer, proposed the following correlation for gas convective heat transfer coefficient.

$$\frac{h_{gc} d_p}{K_g} = 0.017 Ar^{0.46} \Pr^{0.33} \left(\frac{V}{V_{mf}}\right)^{0.3} \tag{67}$$

where Ar is the Archimedes number

$$Ar = \frac{d_p^3 \rho_g^2 g}{\mu^2} \left(\frac{\rho_s - \rho_g}{\rho_g}\right) \tag{68}$$

Their experiments showed that the contribution of the gas convective component to the overall heat transfer increased from 10 to 95 percent when particle diameter was increased from 0.16 mm to 4.0 mm.

Summary of heat transfer calculation from an outer wall of pipe to fluidized bed.

The objective of this section is to summarize how the overall convective heat transfer coefficient from an immersed horizontal tail pipe to a gas fluidized bed can be estimated. The expression obtained was

$$h_{ove} = h_{pc} + h_{gc} \tag{69}$$

The particle convective heat transfer coefficient, h_{pc}, will be obtained from an analytical solution which is based upon the modified packet model. Earlier use described how all unknown values such as the thermal conductivity of emulsion phase $\mathbf{K}_{mf}$, the gas film thickness δ, and the emulsion packet residence time τ can be obtained using equations (57), (60), and (64), respectively. These values can, then, be used to calculate the averaged particle convective heat transfer coefficient using equation (54).

The estimation of the gas convective heat transfer coefficient, h_{gc}, was obtained using Baskakov's semi empirical equation (67). This equation was used to predict the heat transfer coefficients in fluidized beds in previous studies [23,24]. In their investigation, the heat transfer coefficients between constant temperature wall pipe and a similar fluidized bed were measured. Since in the present application, heat transfer to the bed results in an axial temperature gradient along the pipe, this research focused on predicting the heat transfer coefficient for this heat pipe with axial temperature gradient the fluidized beds.

Center line temperatures can be calculated using the assumption that the tail pipe surrounded by an isothermal fluid in case of natural convection in section II-1.4. Alternatively, center line temperature in case of fluidized convection can be calculated by just replacing the external heat transfer coefficient, h_e with h_{tot}. More detailed explanations will be given in next section.

Calculation of the center line temperature

Once the local heat transfer coefficients have been calculated using quasi-steady theory, conservation of energy can be applied to obtain the center line temperature profile.

The enthalpy difference between two axial location 1 and 2 is given by

$$q = \dot{m} C_p (T_{m1} - T_{m2}) \tag{70}$$

The convection heat transfer rate from the hot gas, whose average mean temperature is $T_{m\frac{1}{2}}$, into the wall is expressed as.

$$q = hA_s (T_{m\frac{1}{2}} - T_i) \tag{71}$$

Since these two heat transfer rate must balance we obtain the following equation.

$$q = \dot{m} C_p (T_{m1} - T_{m2}) = hA_s (T_{m\frac{1}{2}} - T_i) \tag{72}$$

Here the values of $\dot{m}$, C_p, T_{m1}, h, A_s and T_∞ are known and those of T_{m2}, $T_{m\frac{1}{2}}$, and T_i are unknown. Since there are too many unknowns to solve the equation another boundary condition must be applied. Since in practical cases neither wall temperature nor the heat flux are not constant it is assumed that heat transfer from the pipe to a surrounding isothermal fluid (e.g., room temperature air) [26,45].

Sparrow and Patankar [45] showed that the wall heat flux varies exponentially in the streamwise direction for all known constant internal and external heat transfer coefficients. This isothermal boundary condition is applied to pipe flow with periodically varying internal heat transfer coefficient.

Figure 6 shows the expected temperature variation along a heat pipe cooled by an isothermal external fluid. Assuming that the external heat transfer coefficient, h_e is known and constant, the local heat transfer rate may be taken as proportional to the ambient-heat pipe temperature difference.

$$q = h_{eff} A_s [T_\infty - T_o(x)] \tag{73}$$

where h_{eff} is the effective external heat transfer coefficient including wall heat conduction.

$$h_{eff} = \left(\frac{r_i}{k_w}\ln\frac{r_o}{r_i} + \frac{r_i}{r_o}\frac{1}{h_e}\right)^{-1} \tag{74}$$

Determining an expression for the enthalpy difference q is complicated by the exponential nature of the temperature decay. Equation (70) can be expressed in the form

$$q = \dot{m}C_p(T_{m1} - T_{m2}) = \dot{m}C_p[(T_{m1} - T_\infty) - (T_{m2} - T_\infty)] = \dot{m}C_p(\Delta T_1 - \Delta T_2) \tag{75}$$

The expression for the convection heat transfer rate (68) then becomes

$$q = h_{tot} A_s \Delta T_{lm} \tag{76}$$

where total heat transfer coefficient h_{tot} can be obtained using the resistance theory and ΔT_{lm} is the log mean temperature difference [46],

$$\frac{1}{h_{tot}} = \frac{1}{h} + \frac{1}{h_{eff}} \tag{77}$$

$$\Delta T_{lm} = \frac{\Delta T_1 - \Delta T_2}{\ln \Delta T_2 / \Delta T_1} \tag{78}$$

Once again, conservation of energy causes the q's in equations (75) and (76) to be equal

$$\dot{m}C_p(\Delta T_1 - \Delta T_2) = h_{tot} A_s \frac{\Delta T_1 - \Delta T_2}{\ln \Delta T_2 / \Delta T_1} \tag{79}$$

Rearranging equation (76) in the form

$$\ln \frac{\Delta T_2}{\Delta T_1} = \frac{-1}{M} \tag{80}$$

where

$$1\ M = \frac{\dot{m}C_p}{h_{tot}} \tag{81}$$

allows the unknown value ΔT_2 to be obtained from the following equation :

$$\Delta T_2 = T_{m2} - T_\infty = (T_{m1} - T_\infty) e^{-1/M} \tag{82}$$

where the mean temperature T_m is converted into center line temperature T_c

$$T_m = 0.9416 T_c \tag{83}$$

Calculation of the inner wall temperature

The inner wall temperature can be obtained using a simple energy balance between the axial enthalpy difference and the inner convective heat transfer rate.

Figure 7 shows the control volume for the heat transfer rate calculation. The inner wall temperature can be calculated using the following equation from the mean temperature variation, which was calculated in the previous section.

$$T_i = T_{m\frac{1}{2}} - \frac{\dot{m}C_p(T_{m1} - T_{m2})}{hA_s} \tag{84}$$

Calculation of the outer wall temperature

The outer wall temperature can be obtained using a simple energy balance between the axial enthalpy difference and conductive heat transfer rate from the inner to the outer walls. From Fourier's law the conduction heat transfer rate can be expressed in the form

$$q = k_w A_s \frac{(T_i - T_o)}{t} \tag{85}$$

Finally, the outer wall temperature can be also be obtained from the following equation using the value of the inner wall temperature, which was calculated previously.

$$T_o = T_i - \frac{\dot{m} C_p (T_{m1} - T_{m2})}{k_w A_s} t \tag{86}$$

Experimental Study of Heat Transfer

Experimental apparatus

A schematic of the developed experimental setup is shown in Fig. 8. A 3 foot long, 1 foot wide, and 3 foot high fluidized bed is filled with sand to a depth of 5.5 inches without fluidization. This permits operation with turbulent fluidization, since the maximum bed expansion has been reported to be about 50-250% of its packed bed height [35]. The height of the plenum is 1 foot.

A Mott porous metal type distributor provides uniform air flow for fluidization. A centrifugal compressor is used to provide fluidization air. A window made from a Lexan plate located in the front wall of the bed is used to check the fluidization condition in the bed. Sand can be removed through the window to provide access to the heat transfer pipe. Fluidizing air is exhausted through the top.

A single heat transfer tail pipe is installed 3 inch above the distributor. To simulate the hot, pulsating flow in a pulse combustor tail pipe, an electrical heater and acoustic drivers are installed in the tail pipe. The temperature of the air flow through the pipe is adjusted by controlling the heater voltage.

An acoustic decoupler separates the test section of the pipe from the heater in order to set a clear acoustic boundary condition. In addition, this decoupler prevents disturbances in the flow due to the coils of the electrical heater from entering the inlet section. Four acoustic drivers, which can provide a maximum sound level of 169 dB in this set-up, are mounted on the downstream end of the tail pipe wall. These acoustic drivers are used to excite a standing axial acoustic wave of adjustable frequency and amplitude in the heat transfer tail pipe to simulate the pulse combustor tail pipe. The acoustic frequency and amplitude are controlled by a function generator accompanied by changes in the length of the heat pipe, in order to maintain resonance.

Temperature and heat flux measurement

The center line temperature of the flow in the tail pipe was measured using a movable 73 inch long, ¼ inch diameter, K-type exposed junction thermocouple. To keep the thermocouple junction centered in the pipe, a special thermocouple support was designed, see Fig. 9. The interior surface temperature of the tail pipe was measured using eroding type Nanmac thermocouples made of carbon steel, which is the same material as the tail pipe. This reduced any influences on the heat transfer process due to different material in the thermocouple. The outer surface temperature of the tail pipe was measured using an Omega washer type thermocouple. A schematic of the entire temperature measurement setup is shown in Fig. 9.

The radial temperature distribution in the pipe at the entrance to the fluidized bed was measured in 1/32 inch intervals using an 1/8 inch diameter, K-type exposed junction thermocouple. Average thermocouple bead diameter is 0.09.inches. The thermocouple was bent into an L shape to minimize the flow disturbance and errors from heat conduction through the thermocouple itself. Figure 11 shows that the radial temperature distribution was symmetric and that the temperature over the central 75% of the cross-section was within 2% of its maximum value. This means that if the thermocouple used to measure the axial temperature distribution moved slightly off the center as it is traversed in axial direction, the resulting error in the recorded temperature was very small. Temperature distributions inside fluidized bed were measured using a

movable 24-inch long, 1/4 inch diameter, K-type exposed junction thermocouple. Fluidized bed temperature was measured horizontally from the side surface of the tail pipe to the fluidized bed wall at 0.5 inch intervals at 5 different axial positions. Fluidized bed temperature was also measured vertically from the fluidized distributor surface to the top of the sand every 0.5 inches.

Heat fluxes from the outer wall to steady air in case of natural convection, and to sand in a fluidized bed in case of forced convection, was measured at selected locations using Omega thin film, heat flux sensors model #HFS-4, respectively. Heat flux sensors were attached to the bottom, side and top of the tail pipe surface using Kapton tape, in order to investigate azimuthal heat transfer coefficients.

Pressure and minimum fluidization velocity measurement

The acoustic pressure oscillations in the tail pipe flow were measured using a specially designed water cooled, pressure probe. The probe, shown schematically in Fig. 10, consists of three concentric stainless steel tubes. Cooling water flows between the outer two tubes to maintain a constant temperature in the center tube. The inner tube is open at the probe tip and attached at the other end to a long tube to minimize the frequency response of the probe. Near the interface between the probe and "semi-infinite tube," a ¼ inch Bruel and Kjaer type 4136 condenser microphone is attached in a T like configuration to measure the pressure signal. An uncooled pressure probe is also used in order to investigate how the water cooled pressure probe affects the standing wave.

Fluidization is the operation by which solid particles are transformed into a fluid-like state through suspension in a gas or liquid. At a certain fluidization velocity of the gas, the frictional force between particles and fluid just counterbalances the weight of the particles. The vertical component of the compressive force between adjacent particles disappears and the pressure drop through any section of the fluid bed equals the weight of fluid and particles in that section. The bed is considered to be just fluidized and is referred to as an incipiently fluidized bed or a bed at minimum fluidization. the pressure difference between the bottom and top of the bed ΔP is measured using manometer. Figure 12 shows the pressure difference between the bottom and top of the bed ΔP vs. fluidization velocity. Minimum fluidization velocity is reached when the curve levels off. Air flow rate entering the fluidized bed was measured using orifice meter. Minimum fluidization velocity was determined from known air flow rate and fluidized bed distributor area. All experimental tests were carried out at 30% above this minimum fluidization velocity condition because the heat transfer inside the fluidized bed has been shown to be maximum at this operating condition [35].

Experimental methodology

In all tests, the apparatus was allowed to run at least two and a half hours to establish thermal equilibrium before any data are recorded. The local heat transfer rate was calculated from the temperature distribution using enthalpy differences at consecutive downstream stations. The mass flow rate $\dot{m}$, specific heat C_p, and the tail pipe surface area A_s are known. The bulk mean temperatures at each station, T_{m1}, T_{m2}, and the average bulk temperature in between the stations $T_{m_{\frac{1}{2}}}$ are measured using the center line temperature probe. The inner wall temperature T_i was measured using the wall temperature probe. The conservation of energy states that the local heat transfer rate $\dot{m}C_p(T_{m1} - T_{m2})$ must be equal to the convective heat transfer rate $hA_s(T_{m_{\frac{1}{2}}} - T_i)$ between the hot flow and the interior wall of heat transfer tail pipe, i.e.,

$$q = \dot{m}C_p(T_{m1} - T_{m2}) = h_i A_s(T_{\frac{1}{m_2}} - T_i) \tag{87}$$

The local heat transfer coefficient can then be expressed by

$$h_i = \frac{\dot{m}C_p(T_{m1} - T_{m2})}{A_s(T_{\frac{1}{m_2}} - T_i)} \tag{88}$$

Which was used to calculate the local heat transfer coefficient h_i and the Nusselt number.

For each run the temperature of the flow at the location where the pipe enters the fluidized bed, is set to the same value in order to keep the enthalpy entering the "control volume" constant. Tests are then run with and without pulsation and the axial center line temperatures are measured at 3 inch intervals over the length of the pipe immersed in the fluidized bed.

Results and Discussion

Figure 13 shows the heat transfer distribution in the axial direction without pulsation. It was found to be about 15 J/sec near the center of the tail pipe, and about10 J/sec higher near the walls containing the fluidized bed. The acoustic drivers at the downstream end of the tail pipe were then turned on and tuned to 456 Hz which corresponds to one of the resonance frequencies of the pipe. The maximum sound pressure level in the pipe that could be produced at this operating condition was 164 dB. Heat transfer rate with acoustic pulsations varied periodically along the length of the pipe between 40 J/sec and 15 J/sec. These heat transfer oscillations have a wavelength that is about one half that of the standing wave of the acoustic pressure in the pipe, see Fig. 14.

The downstream end of the tail pipe was modified by adding a cap that acts as a muffler. This allowed the sound pressure level in the pipe to be increased to 166 dB. At the same time, the acoustic drivers were tuned to a different resonance frequency of the pipe at 282 Hz. Figure 15 shows measured center line temperatures both without and with pulsations with error bars which indicate the maximum deviation of each temperature measurement from their averaged value at every measuring position. This clearly indicates that the data is fully repeatable. This data repeatability is very important because observed fluctuations in heat transfer rates are due to very small fluctuations in axial temperature. Figure 16 shows the error bars for the heat transfer rates calculated from the temperature data in Fig. 15. Clearly the locations of minimum and maximum heat transfer are not affected by these measurement errors which are, at most, of the order of 20%. The results in Fig. 16 show a similar variation of the heat transfer rate in the downstream direction as those in Fig. 14, except that the wave length of this variation is now scaled proportionally to that of the new standing acoustic wave, see Fig. 17. In addition, the higher sound pressure levels result in higher heat transfer rates. The larger pulsations increase the mean heat transfer rate by about 60% over those without pulsation.

Figure 19 shows the local heat transfer rates along the tail pipe of the simulated pulse combustor at a higher frequency, 389 Hz. At the center area of the tail pipe, the maximum heat transfer rate occurred at the pressure node; i.e., at the velocity anti-node. That is to say the velocity fluctuation is spatially in phase with that of the heat transfer rate. However, this correspondence is no longer observed near the wall of the fluidized bed. It was suspected that this discrepancy was caused by large heat losses to these walls.

In order to test the above hypothesis, the pipe was removed from the fluidized bed. Tests were carried out with only natural air convection removing heat from the outside surface of the tail pipe and no heat loss to the fluidized bed walls. Under these conditions the local heat transfer rate measurements were repeated for several different Reynolds numbers. The results were similar to those obtained when the tail pipe was attached to the walls of the fluidized bed. The maximum heat transfer rates once again coincided with the velocity anti-nodes near the central area of tail pipe. However, at the two ends of the pipe, the heat transfer and acoustic velocity fluctuation were spatially out of phase. Thus, the presence of the fluidized bed walls did not cause the observed effect.

Another reason for the mismatch between heat transfer and the acoustic velocity anti-node needed to be found. Inspection of the pipe revealed a 1/8 inch groove where the flanges were fitted to the fluidized bed wall or to each other. It was deemed that this groove caused a boundary layer breakdown, which changed the rate of heat transfer. To test this hypothesis, heat transfer measurements were carried out using a smooth pipe with no flange connections. Figure 18 shows the heat transfer rate variations along the axis in the smooth pipe. Clearly, the spatial heat transfer rate fluctuations are now 180° out of phase with the pressure node not only in the central region of tail pipe but along the entire pipe. Thus, it appears that the presence of grooves in the wall of heat transfer pipes definitely affects the local heat transfer rates in the presence of pulsations.

Local heat transfer coefficients and then, Nusselt numbers were also determined. The inside tail pipe wall temperatures were measured using the Namac thermocouple described above. Figure 19 shows the axial value of the Nusselt number determined from experiment and from theory using Equation 3 for flow without pulsations. At the upstream end of the tail pipe, the calculated Nusselt number is much smaller than the corresponding experimental values, because theory cannot predict the entrance effect, i.e., the boundary layer growth upstream. Further downstream the calculated values are more close to those measured because the disturbance effect of flange gap diminishes in this region. Previous tests have shown that a turbulent flow becomes hydrodynamically and thermally fully developed after a relatively short distance (10 diameters) from the entrance to a pipe [26]. This full development criterion is particularly applicable to fluids with Prandtl numbers of order 1 and RE > 2000. It is therefore, reasonable to assume that the flow in the test section is hydrodynamically and thermally fully developed because the experimental test section begins 19.2D away from the entrance of the pipe. Figure 19 shows that above assumption is correct since the measured Nu numbers in a pipe without flange are very close to those of calculated.

Figure 20 compares the Nusselt number obtained experimentally with that calculated using quasi steady theory for the case of flow with pulsations using Equation 8. At both upstream and downstream ends of the tail pipe, the experimental Nusselt numbers of tail pipe with flange do not match the corresponding calculated values. This may be due to the boundary layer breakdown caused by the flange. There is less than a 20% difference between those two Nusselt numbers in the central region. This spatial phase mismatch between experiment and theory is very small throughout the pipe without flange.

Comparisons of heat fluxes from tail pipe immersed in fluidized bed:

The experiments reported in this section were carried out for forced convection, i.e., inside fluidized bed. Figures 21 and 22 show a comparison of heat transfer rates calculated from the measured enthalpy differences and those measured directly using a heat flux probe placed on the extended wall o f the pipe at various axial locations with and without pulsation, respectively.

Q1, Q2 and Q3 are heat transfer rates from the top, the side, and the bottom of the tail pipe to the surroundings, respectively. Q3 has highest heat transfer rate since boundary layer at lateral side is narrowest in natural convection. Q1 and Q2 have lower heat transfer rates because stagnation points locate on the top and bottom of the tail pipe.

Closer inspection of Figs. 21 & 22 reveals that the heat transfer at the side of the pipe (Q2) dominates the process. Heat transfer near the stagnation points (Q1) is minor and exerts an undue influence on the total heat transfer rate (Q3). In addition, the difference between the heat transfer rate measured by enthalpy difference and that measured directly using a heat transfer probe is due to the fact that the former is determined at the inner wall of the pipe while the latter is measured at the outer wall. This suggests a high lateral rate of heat transfer in the pipe wall.

Figures 23 and 24 show a comparison between the calculated and measured values of the axial temperature distribution of the outer wall of the pipe without and with pulsations, respectively. These temperature distributions are comparatively flat because of the high heat transfer rate to the fluidized bed. It is also noticed that the theory under predicts the out wall temperature by about 10° K (approximately 3%) in all cases.

Figures 25 & 26 show comparisons of the measured and calculated Nusselt numbers along the axis of the pipe submerged inside the fluidized bed, with and without pulsation, respectively. Figure 25 shows theory and measured Nusselt numbers in good agreement. However, the differences between calculated and measured Nusselt numbers with pulsations flow inside fluidized bed are much larger. Nevertheless, the theory still predicts the exact minimum and maximum Nusselt number locations.

The degree of heat transfer rate enhancement is defined as the ratio of the overall value of the heat transfer rate with pulsations tot hat without pulsations. Figure 27 shows Nusselt number enhancement while varying the ratio of acoustic velocity to mean velocity as predicted by the quasi-steady theory. The Nusselt number actually decreases a little until the velocity ratio is 1 and then rapidly increases. Figure 28 shows the experimentally determined degree of heat transfer rate enhancement which clearly follows the same trend.

Some light can be shed on the mechanism that caused the enhanced heat transfer in the presence of pulsations by comparing the radial temperature distribution, with and without pulsation in the pipe, see Fig. 29. At low Reynolds number (RE=3,200) the temperature profile with pulsation is clearly fuller than that without pulsation. Thus, the acoustic pulsations steepen the temperature gradient next to the pipe wall, which increases heat transfer rate. Figure 30, on the other hand, shows a similar comparison for a Reynolds number of 13,400. Here there is little difference between temperature profiles with pulsation and without pulsation. This explains why the effect of the pulsations on heat transfer is less pronounced in turbulent flow.

Heat transfer in fluidized bed

Figure 31 shows temperature distribution of the fluidized bed along a vertical axis through the tail pipe, which is located 60 cm above the distribution plate. The temperature above the tail pipe is almost constant. The bed temperature with pulsations is about 50K higher than without, indicating that the pulsations have some limited effect. Figures 32 and 33 show the fluidization bed temperature distribution along the lateral direction from the tail pipe wall. Clearly, the temperature is higher with pulsations than without. However, the effect is short lived since less than an inch from the wall the bed temperature has dropped to that without pulsations.

The above observations suggests that heat transfer from the exhaust gases in the pipe to the pipe wall is the controlling step which, if enhanced, can lead to a heat buildup on the outer surface of the pipe.

Thus the pulsations inside the tailpipe do enhance the heat transfer to the bed. However, much of this is caused by the reduced fluidization near the pipe. Further away from the pipe, heat transfer in the bed is fast enough to keep the Reynst distribution uniform.

CONCLUSIONS

This project had two goals. The first was to determine whether the products of the pyrolysis of black liquor can be used to fire a pulse combustor. Furthermore it was investigated whether the pulsations generated in the tail pipe of a pulse combustor, submerged in a fluidized bed, can enhance the heat transfer from the combustor exhaust gases to the bed without generating 'hot spots'.

During the first part of the investigation it was determined that changes in heat content do not have a marked effect on the sound pressure level in the pulse combustor as long as the only combustible in the fuel is methane. However, hydrogen in the fuel advances the timing of the heat release during the cycle. In agreement with Rayleigh's criterion, this leads to reduced driving and thus, lowers amplitudes and increased frequency in the combustor. Hydrogen in the fuel also causes the dB level in the combustor to decrease with increase in heat content. Tests in which the fluid mechanics in the combustor was kept constant while the composition of the fuel was changed have indicated that the changes in combustion chemistry rather than mixing rates are responsible for these observations. Finally, it was determined that while the addition of hydrogen to the methane fuel reduces the amplitude of the pulsations, the increase in combustion rate significantly extends the rich limit of operation of the pulse combustor by accelerating the combustion process.

Pulsations were shown to increase the overall heat transfer from the exhaust gases of the pulse combustor through the tail-pipe to the fluidized bed as long as the acoustic velocity on the pipe was greater than the mean velocity of the flow; i.e., as long as there was flow reversal during part of the cycle. In the presence of pulsations the heat transfer rate from the hot gases to the tail pipe varied along the pipe. Heat transfer was highest at velocity anti-nodes (pressure nodes). However, the thermal conductivity along the pipe appears high enough to avoid fluctuations outside wall temperatures along the pipe. The quality of the inside finish of the pipe has a considerable influence on the heat transfer enhancement by the pulsations. Small grooves on the inner wall disturb the boundary layer sufficiently to affect the actions of the acoustics.

Measurements of the temperature distributions in the pipe with and without acoustics have suggested that the increase in heat transfer with pulsations is caused by a corresponding widening of the temperature profile in the pipe. This moves the hot gases closer to the pipe wall and increases heat transfer.

Temperature measurements in the fluidized bed have shown that the pulsations increase the heat losses from the hot exhaust gases sufficiently to increase the bed temperature in the immediate vicinity of the pipe. However, a short distance away from the pipe the intense stirring of the bed has spread the heat so that little of the enhanced heat transfer remains noticeable. It thus appears that the pulsations do increase heat transfer to the bed. However care must be taken that no hot spots occur immediately next to the heat pipe.

In addition to the above experimental work a theoretical approach based on a quasi steady assumption was used to model the heat transfer in the system. The theoretical results were in good agreement with the experimental data for steady operation. However, in the presence of pulsations the agreement was qualitatively good but quantitatively only fair. A Ph.D. student is currently continuing to investigate these discrepancies as part of his thesis work.

REFERENCES

[1] Mansour, M.N., Duria-Swamy, K. and AghaMohammadi, B., "Pulsed Combustion Process for Black Liquor Gasification", Second Annual Report, DOE/CE/40893-T2, 1993.

[2] Fedorov, B.N., Juzherno - *Fisicherkii Zhurnol*, vol. 32, no. 1, 1977, pp. 167-180.

[3] Zinn, B.T., "Pulsating Combustion", *Advanced Combustion Methods*, Academic Press Inc. (London) Limited, 1986, pp. 113-181.

[4] Jones, H.R.N. and Leng, J., *Combustion and Flame*, vol. 99, 2, 1994, pp. 404-412.

[5] Keller, J.O. and Westbrook, C.K., *Proceedings Twenty-first (Int'l)) Symposium on Combustion*, 1986, pp. 547-555.

[6] Lord Rayleigh, *The Theory of Sound*, Vol. II, Dover, 1945, pp. 224-235.

[7] Keller, J.O., Bramlette, T.T., Dec, J.E. and Westbrook, C.K., *Combustion and Flame*, 75, 1989, pp. 33-44.

[8] Ku, S.H., "An Investigation of the Gas fired Pulsating Combustor," Ph.D. Thesis, School of Aerospace Engineering, Georgia Institute of Technology, August 1988.

[9] Tang, Y.M., Waldherr, G., Jagoda, J.I. and Zinn, B.T., *Combustion and Flame*, Vol. 100, 1/2, 1995, pp. 251-261.

[10] Kreyszig, E., *Advanced Engineering Mathematics*, Wiley Eastern Ltd., 5th Edition, 1985.

[11] Tang, J.M., Ku, S.H., Daniel, B.R., Jagoda, J.I. and Zinn, B.T., *Proceedings 23rd Symposium (Int'l) on Combustion*, 1990, pp. 1005-1010.

[12] Hanby, VI., "Convective Heat Transfer in a Gas-fired Pulsating Combustor," *ASME J. of Engr. for Power*, Vol. 91, pp. 48-52, 1969.

[13] Alhaddad, A. A. and Coulman, G. A., "Experimental and Theoretical Study of Heat Transfer in Pulse Combustion Applications," GRI 82/009.2, Atlanta, GA, March 1982.

[14] Liao, N. S., Wang, C. C. and Hong, J. T., "An Investigation of Heat Transfer in Pulsating Turbulent Pipe Flow," ASME 23rd national Heat Transfer Conference, Denver, CO, 1985.

[15] Keil, R. H. and Baird, M. H. I., "Enhancement of Heat Transfer by Flow Pulsation," Ind. Chem. Process Des. Develop., Vol. 10, 1971.

[16] Gaslitseyskiy, B. M. and Ryzhov, Y. A., "Heat Transfer in Turbulent Gas Flows in the Case of High Frequency Pressure Fluctuations," Heat Transfer-Soviet Research, Vol. 9, No. 4, July-Aug. 1977.

[17] Dec, J. E. and Keller, J. O., "Pulse Combustor Tail Pipe Heat Transfer Dependence on Frequency, Amplitude and Flow Rate," Sandia Rpt. 1988.

[18] Jackson. T. W., Purdy, K. R. and Oliver, C. C., "The Effect of Resonant Acoustic Vibration on the Nusselt Numbers for a Constant Temperature Horizontal Tube," 2nd International Heat Transfer Conference, 1961.

[19] Gel'perin, N. I. and Ainstein, V. G., "Heat Transfer in Fluidized Beds," *In Fluidization*, Academic Press, 1971.

[20] Berg, B. V. and Baskakov, A. P., "Investigation of Local Heat Transfer between a Fixed Horizontal Cylinder and a Fluidized Bed," *International Chemical Eng.*, Vol. 14, No.3, 1974.

[21] Newby, R. A. and Keairns, D. L., "Fluidized Bed Heat Transfer between Parallel, Horizontal Tube-Bundles," *Fluidization*, Cambridge University Press, 1978.

[22] Grewal, N. S. and Saxena, S. C., "Heat Transfer between a Horizontal Tube and a Gas-Solid Fluidized Bed," *J. of Heat and Mass Transfer*, Vol. 23, pp. 1505-1519, 1980.

[23] Clement, I. A., "Heat Transfer in Horizontal Tubes Immersed in Fluidized Beds," Ph.D. Thesis, West Virginia University, 1982.

[24] Suarez, E., "Instantaneous Azimuthal and Average Heat Transfer Coefficient for a Horizontal Submerged in a Mixed Particle Size, Gas-Fluidized Bed," Ph.D. Thesis, Clemson University, 1983.
[25] Dittus, P. W. and Boelter, L.M.K., "Heat Transfer in Automobile radiators of the Tubular type," Int. Comm. Heat Mass Transfer, Vol. 12, 1985.
[26] Bejan, A., *Convective Heat Transfer* 2nd Edition, Wiley & Sons, Inc.,1995.
[27] Martinelli, R. C., Boelter, L.M.K. and Yakahi, S., **"Heat Transfer to a Fluid Flowing Periodically a Low Frequencies in a Verticle Tube,"** *ASME Trans.*, Vol. 65, 1943. ????
[28] Churchill, S. W. and Chu, H.H.S., "Correlating Equations for Laminar and Turbulent Free Convection from a Vertical Surface," *Int. J. Heat Mass Transfer*, Vol. 18, 1975.
[29] Davidson, J. F. and Harrison, D., *Fluidization*, 2nd Edition, Academic Press, 1985.
[30] Botterill, J.S.M., *Fluid-Bed Heat Transfer*, Academic Press, 1975.
[31] Mickely, H. S. and Fairbanks, D. F., "Heat Transfer to Surface Immersed in Fluidized Beds," *AICHE J.*, Vol. 1,1 955.
[32] Xavier, A. M. and Davidson, J. F., "Heat Transfer to Surface Immersed in Fluidized Beds, Particularly Tube Arrays," Fluidization Processing of 2nd Eng. Foundation Conference, 1978.
[33] Kunni, D. and Levenspiel, O., *Fluidization Engineering*, John Wiley & Sons, 1969.
[34] Carslaw, H. S. and Jaeger, J. C., *Conduction of Heat in Solids*, 2nd Edition, University Press, 2nd, 1959.
[35] Mori, S. and Wen. C. Y., "Estimation of Bubble Diameter in Gaseous Fluidized Beds," *AICHE J.*, Vol. 21, No. 1, 1975.
[36] Swift, D. L., "The Thermal conductivity of Spherical Metal Powders Including the Effect of an Oxide Coating," *Int. J. Heat Mass Transfer*, Vol. 9, 1966.
[37] Krupiczia, R., "Analysis of Thermal Conductivity in Granular Materials," Int. Chem. Eng., Vol. 7, 1967.
[38] Zarbrodsky, S. S., *Hydrodynamics and Heat Transfer in Fluidized Beds*, MIT Press, Cambridge, 1966.
[39] Botterill, J.S.M. and Williams, J. R., "The Mechanism of Heat Transfer to the Gas Fluidized Beds," Trans. Inst. Chem. Eng., Vol. 41, 1963.
[40] Botterill, J.S.M. and Desai, M., "Limiting Factors in Gas Fluidized Bed Heat Transfer," Powder Technology, Vol. 6, 1972.
[41] Ozkaynak, T. F. and Chen, J. C. "Average residence Time of Emulsion and Void Phase at the Surface of Heat Transfer Tubes in Fluidized Beds," AICHE. Symp. Series, Vol. 74, 1978.
[42] Cranfield, R. R. and Geldart, D., "Large Particle Fluidization," Chem. Eng. Sci., Vol. 74, 1974.
[43] Gabor, J. D., "Wall-to-Bed Heat Transfer in Fluidized Beds," AICHE. J., Vol. 18, 1972.
[44] Baskakov, A. P., Berg, B. V. and Vitt, O. K., "Heat Transfer to Objects Immersed in Fluidized Beds," Powder Technology, Vol. 8, 1973.
[45] Sparrow, E. M. and Patankar, "Relationship among Boundary Conditions and Nusselt Numbers for Thermally Developed Duct Flow," *J. Heat Transfer*, Vol. 99, 1977.
[46] Incropera, F. P. and Dewitt, D. P., *Fundamental of Heat and Mass Transfer*, 3rd Edition, John Wiley & Sons, 1990.

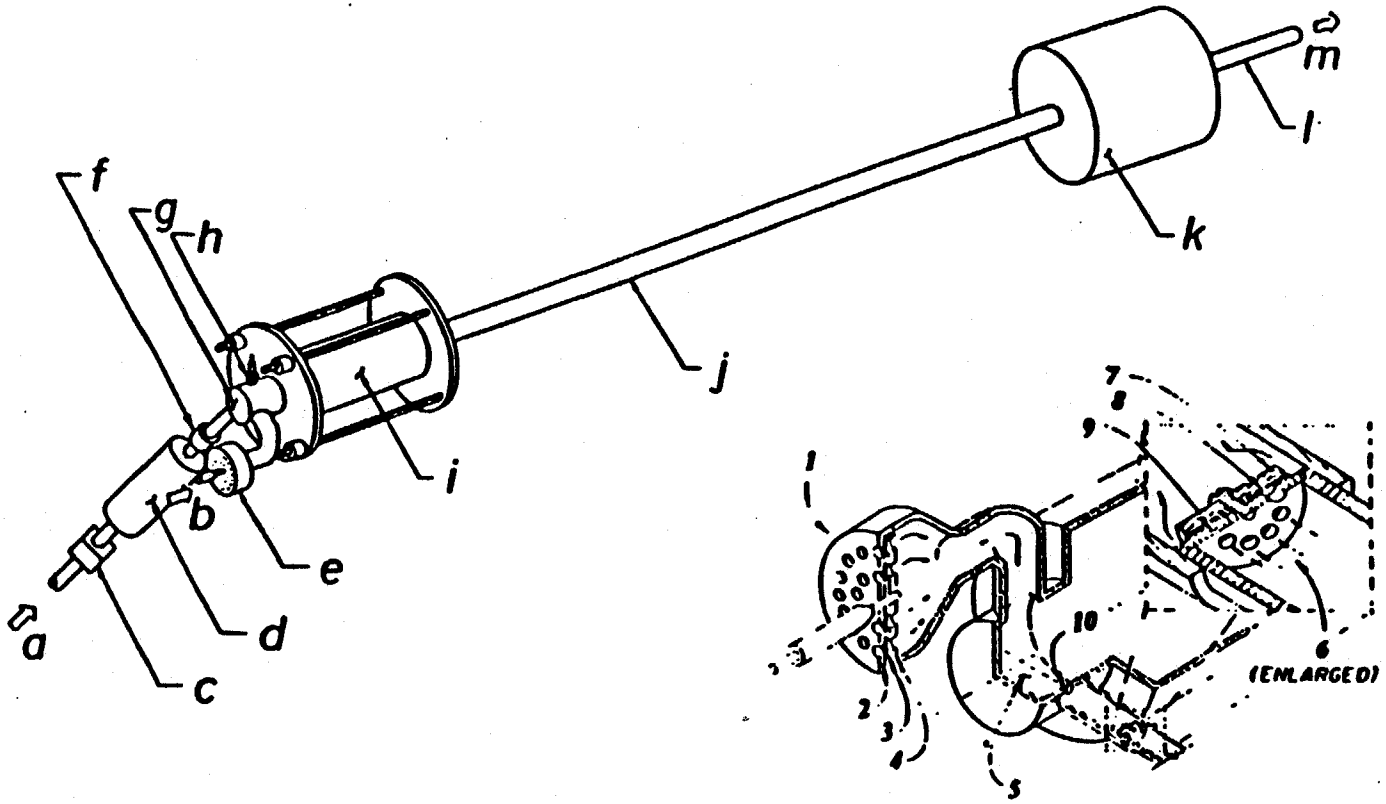

FIG. 1. Schematic of the pulse combustor; a, fuel supply; b, air inlet; c, fuel solenoid valve; d, fuel decoupler; e, air flapper valve; f, fuel flapper valve; g, mixing chamber; h, spark plug; i, combustion chamber; j, tail pipe, k, decoupler; 1, vent pipe; m, exhaust. Cut away: 1, air valve; 2, front plate; 3, flapper; 4, back plate; 5, mixing chamber; 6, fuel valve; 7, back plate; 8, flapper; 9, front plate; 10, fuel orifice.

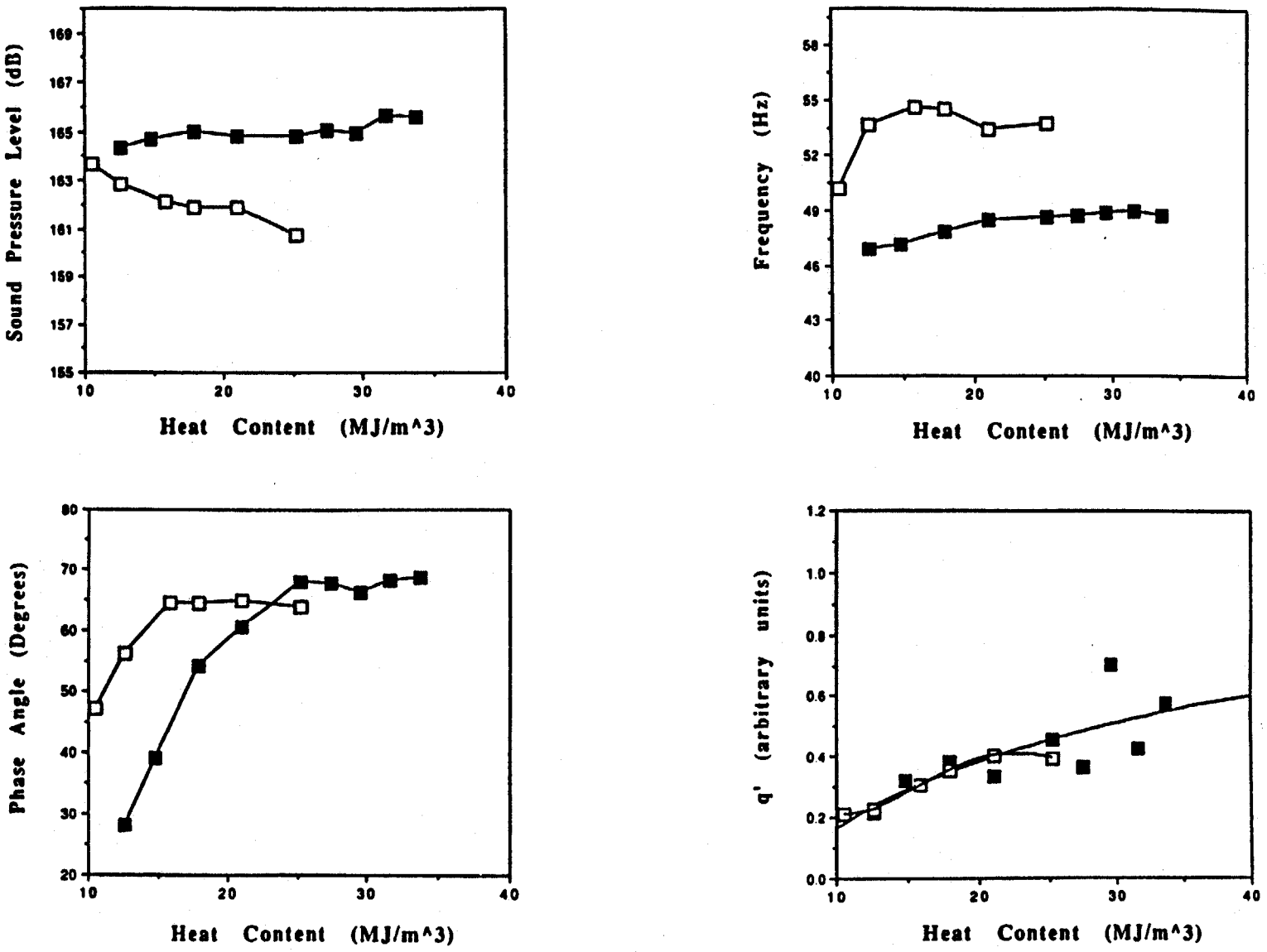

FIG. 2. (a), Dependence of sound pressure level on heat content of the fuel for (■) methane, and (□) methane-hydrogen-based fuels. (b), Dependence of frequency on heat content of the fuel for (■) methane, and (□) methane-hydrogen-based fuels. (c), Dependence of phase angle on heat content of the fuel for (■) methane, and (□) methane-hydrogen-based fuels. (d), Dependence of heat release amplitudes on heat content of the fuel for (■) methane, and (□) methane-hydrogen-based fuels.

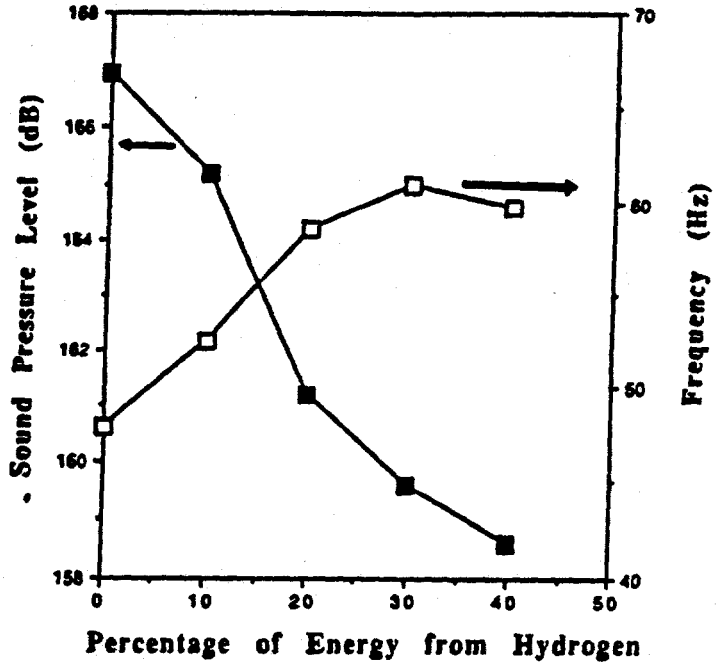

FIG. 3. Dependence of sound pressure level (■), and pulsation frequency (□), on hydrogen content (by percent of heat supplied) in the fuel.

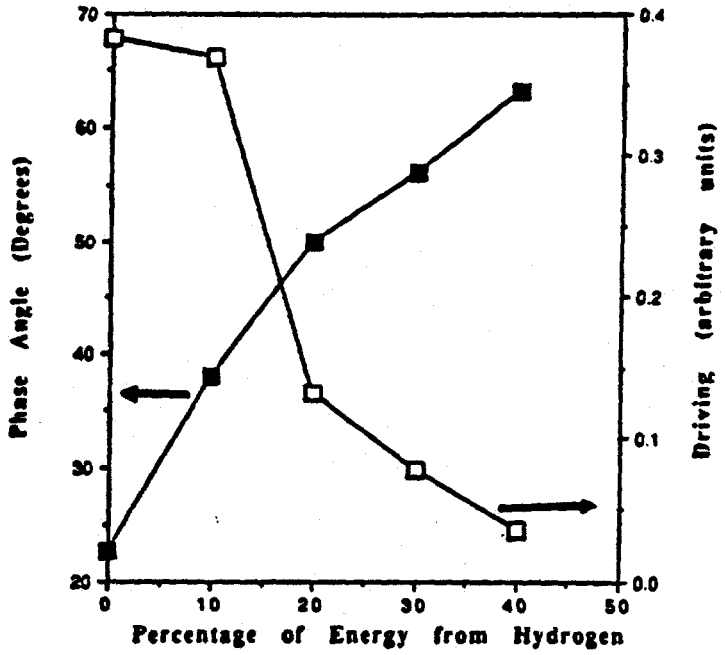

FIG. 4. Dependence of phase angle (■), and acoustic driving (□), on hydrogen content (by percent of heat supplied) in the fuel.

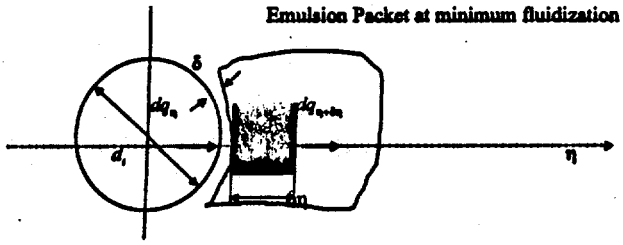

Figure 5: Heat transfer model showing interaction between emulsion packet and pipe

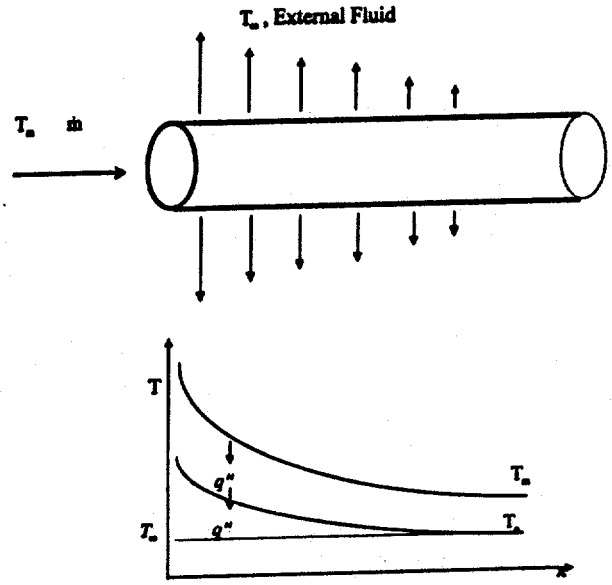

Figure 6: Temperature distribution along the pipe surrounded by an isothermal fluid

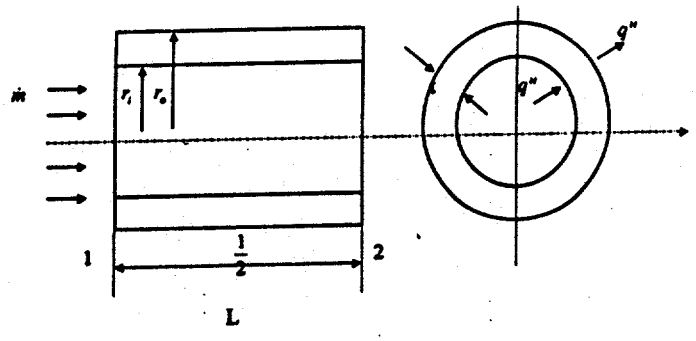

Figure 7: Control volume between axial locations 1 and 2.

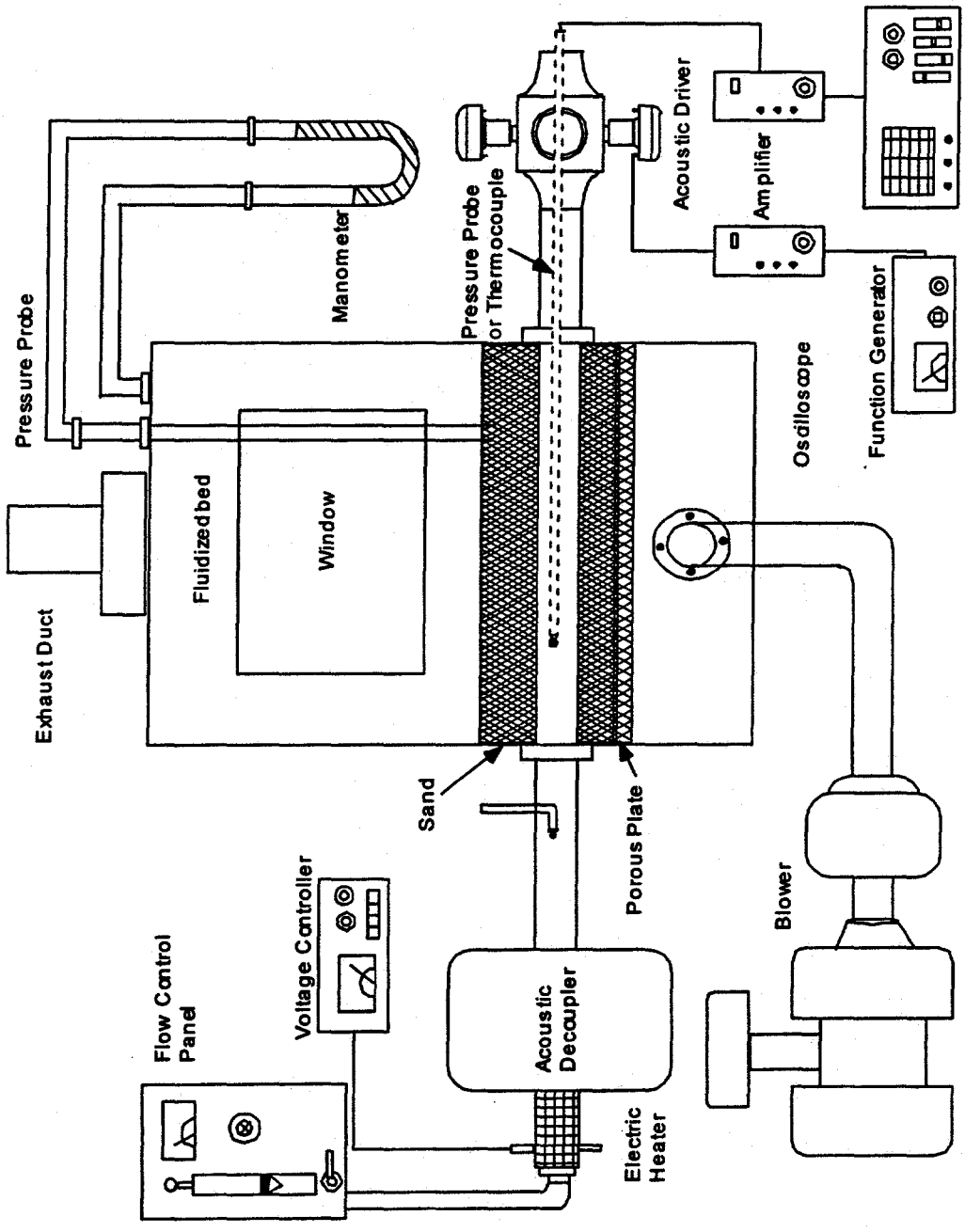

Figure 8: Schematic of experimental setup

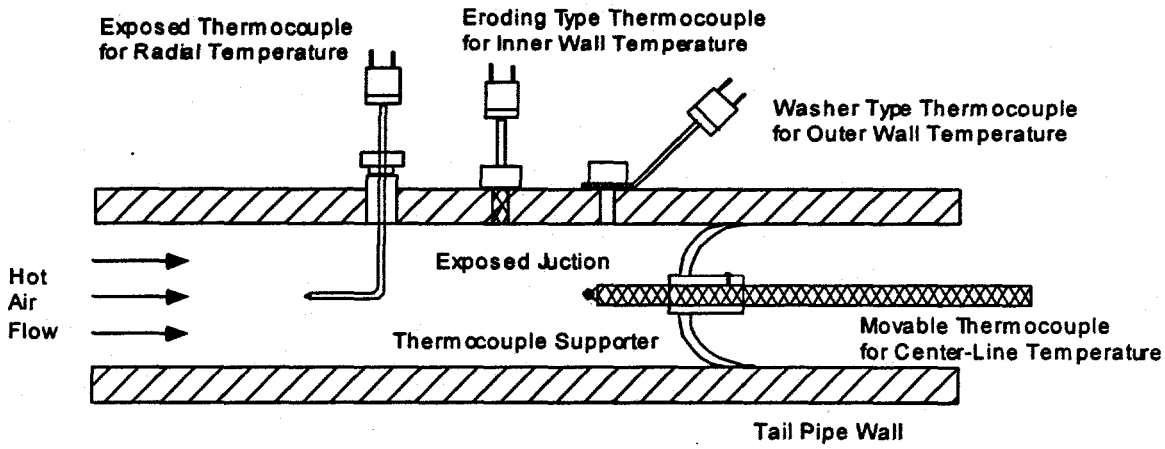

Figure 9: Schematic of temperature measurement setup

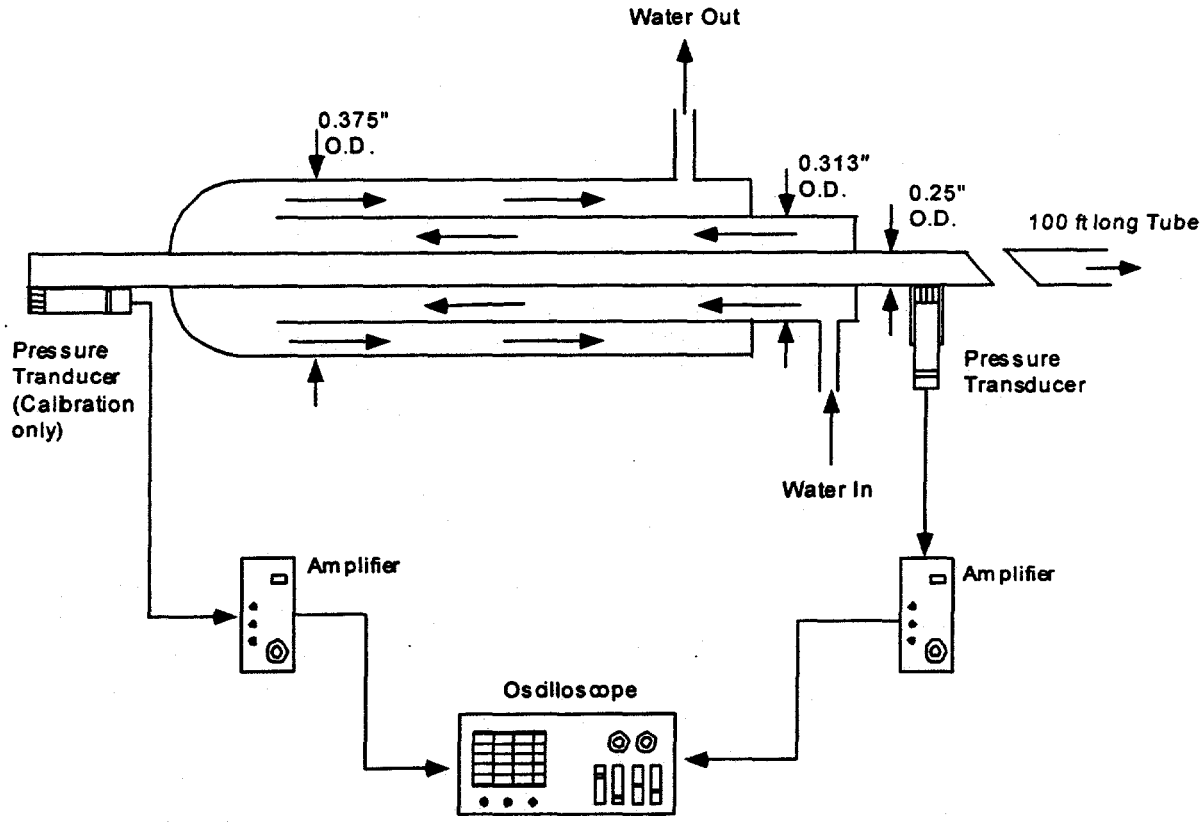

Figure 10: Schematic of water cooled pressure probe

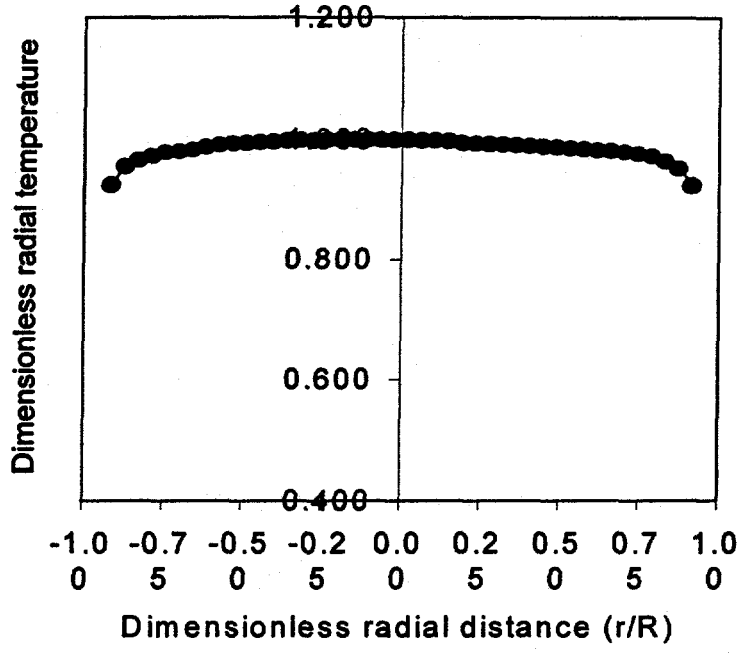

Figure 11: Radial temperature distribution, Re=2050, f=368 Hz.

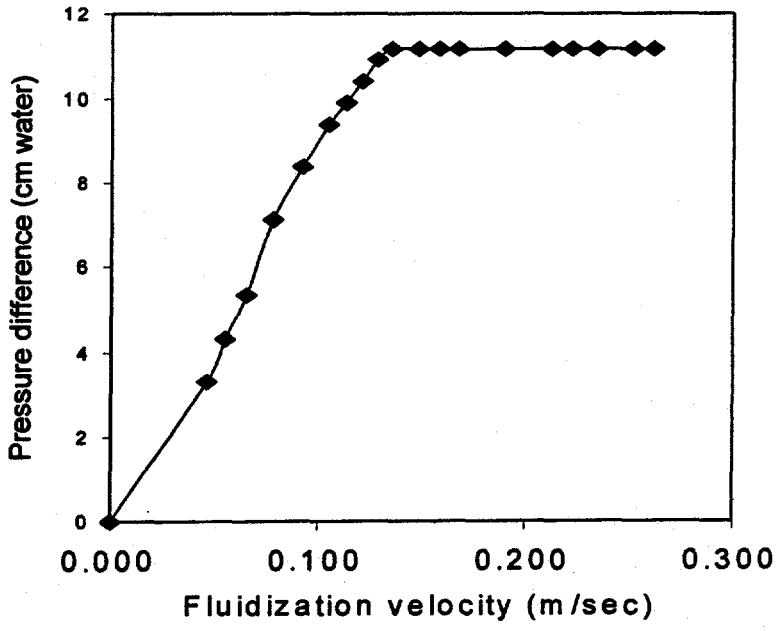

Figure 12: Minimum fluidization velocity

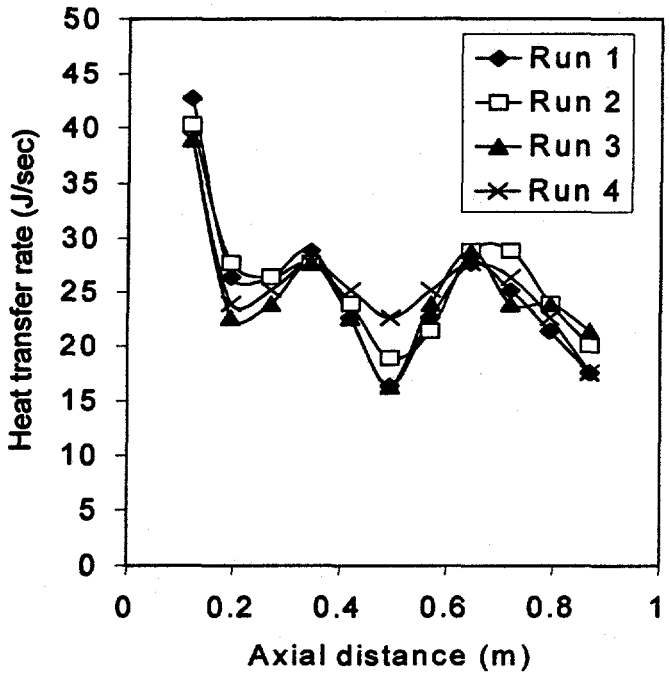

Figure 11: Radial temperature distribution, Re=2050, f=368 Hz.

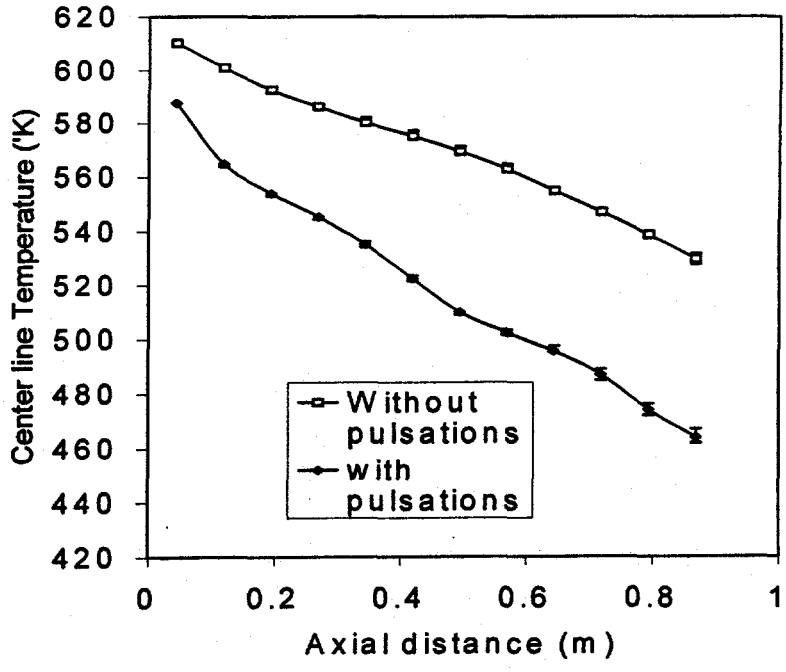

Figure 12: Minimum fluidization velocity

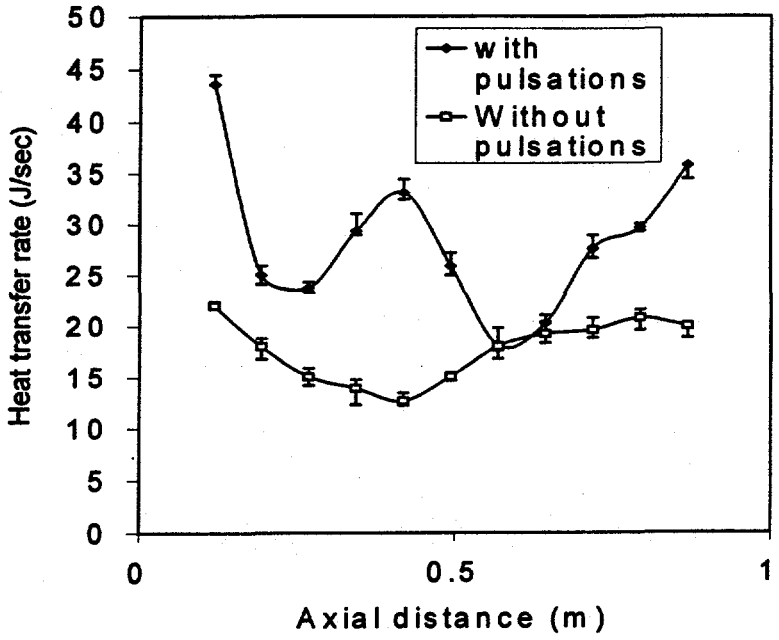

Figure 13: heat transfer rate distribution without pulsations, Re=2500

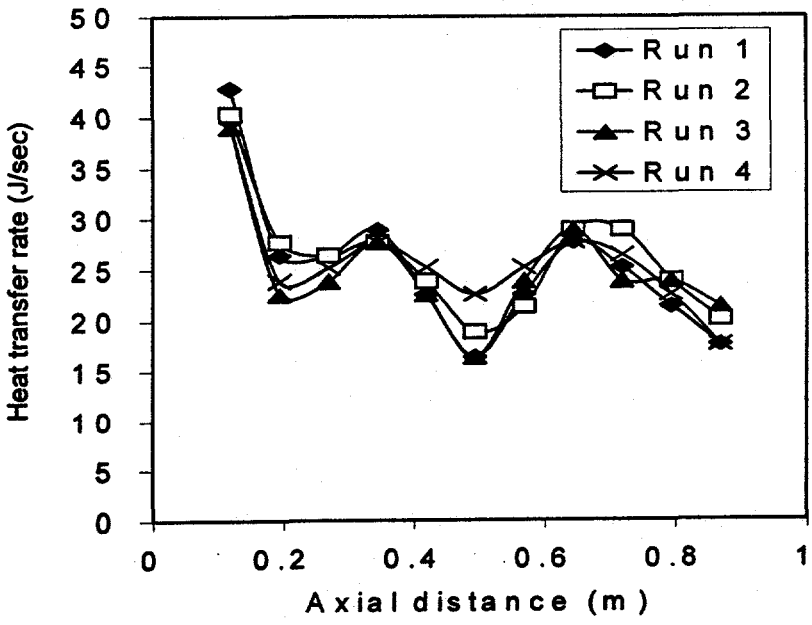

Figure 14: Heat transfer rate distribution with pulsations, Re=2500, f=456 Hz.

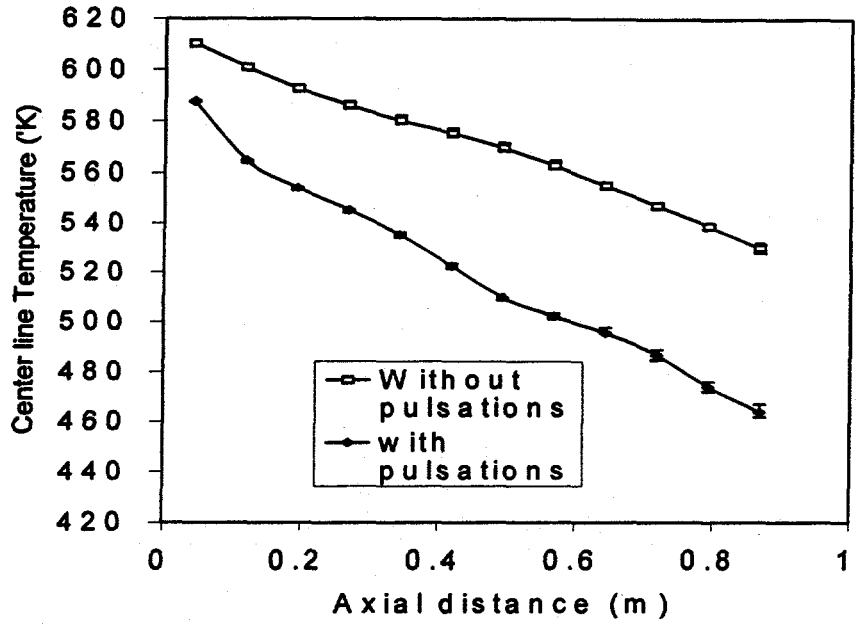

Figure 15: Average center line temperature distributions with error bars, Re=2500, f=282 Hz.

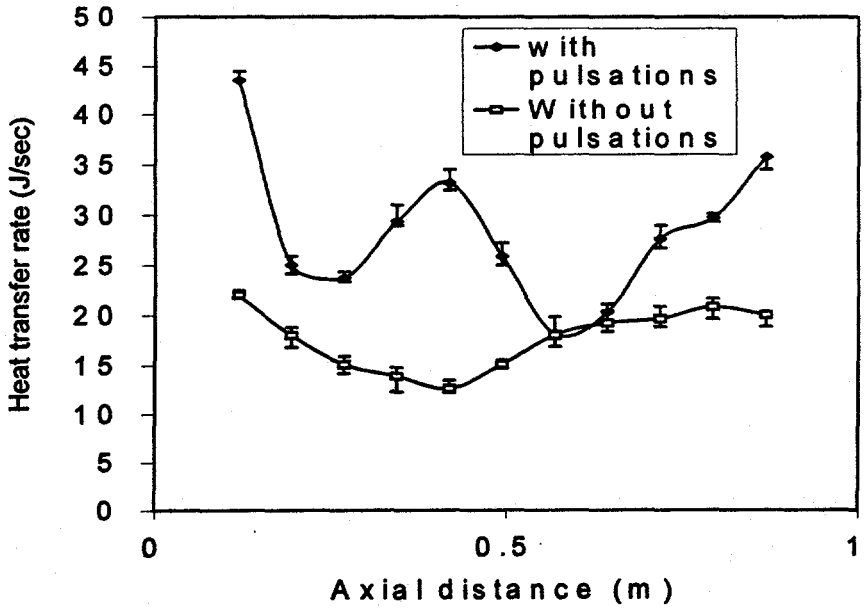

Figure 16: Heat transfer rate distributions with error bars, Re=2500, f=282 Hz.

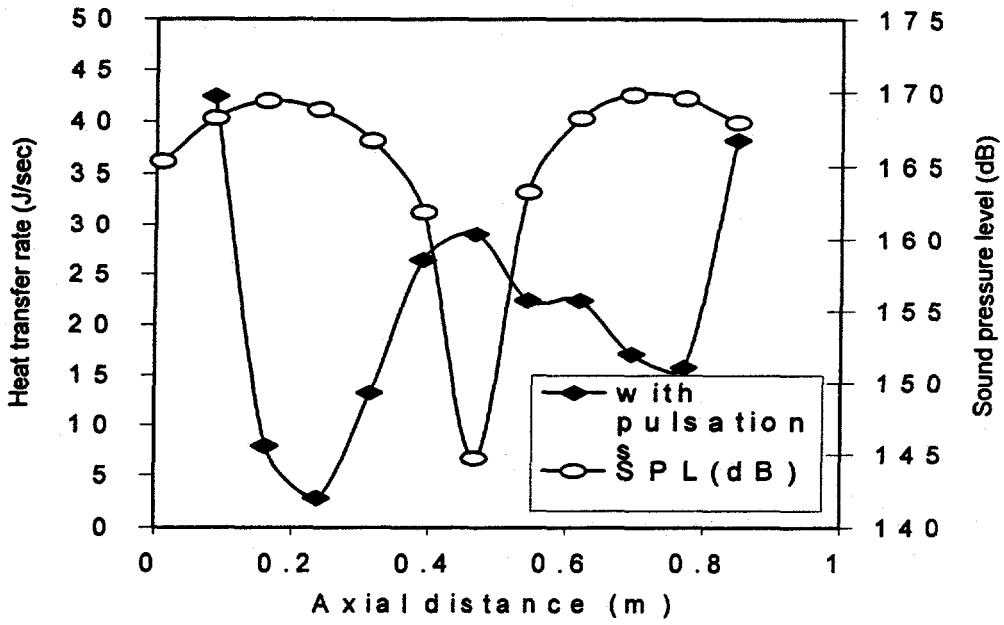

Figure 17: Heat transfer rate distribution, Re=3200, f=389 Hz.

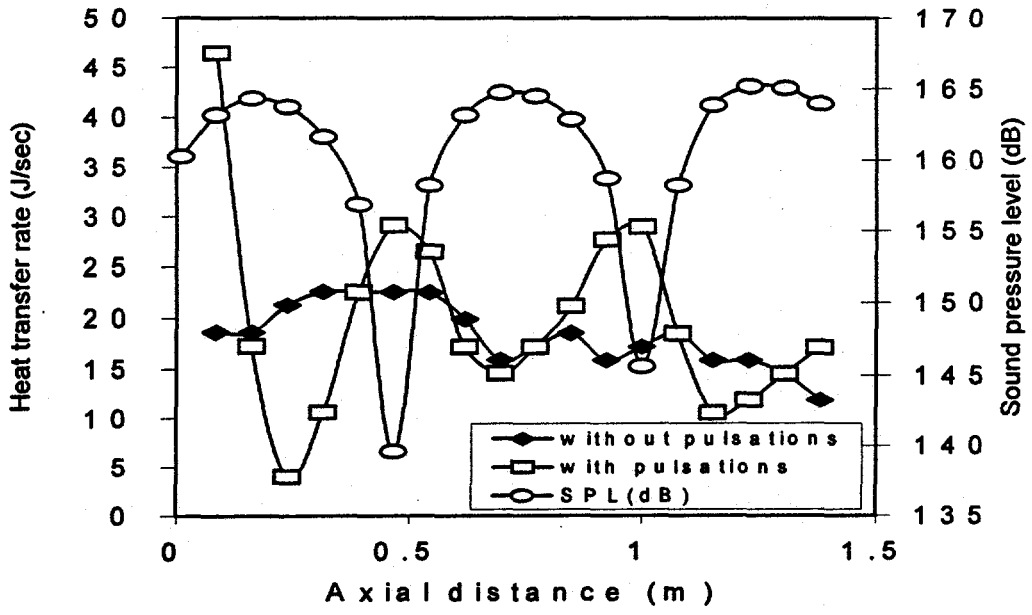

Figure 18: Heat transfer rate distributions in tail pipe without flange, Re=3200, f=389 Hz.

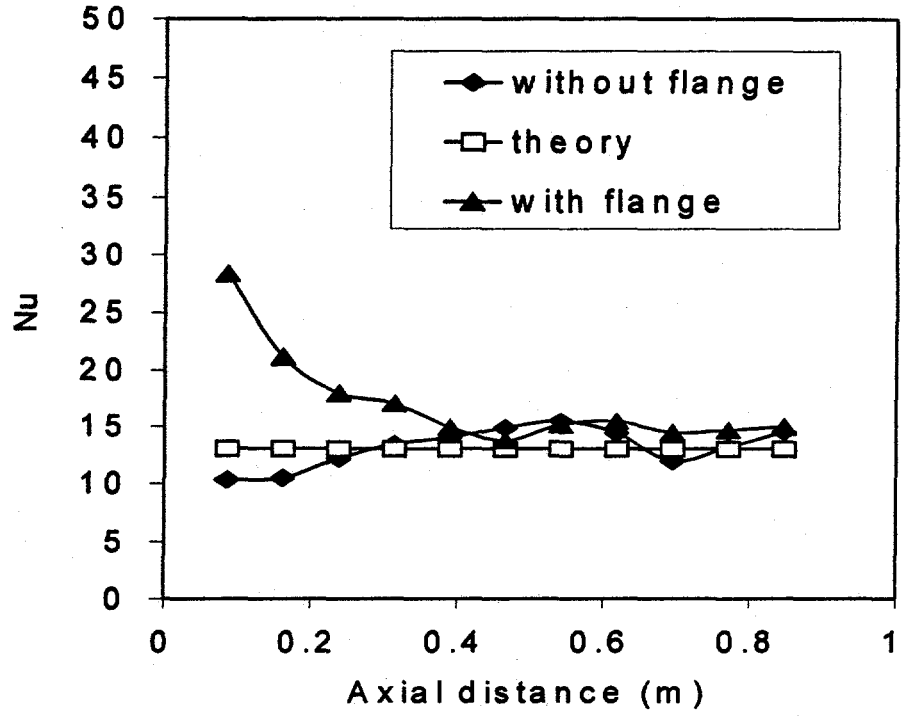

Figure 19: Nusselt number distributions without pulsations, Re=3200, f=389 Hz.

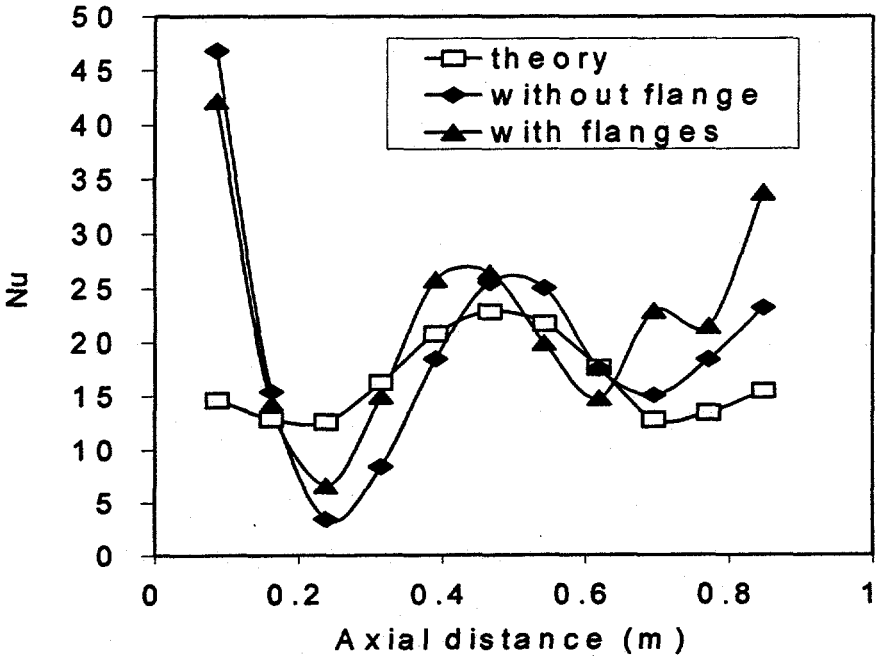

Figure20: Nusselt number distributions with pulsations, Re=3200, f=389 Hz.

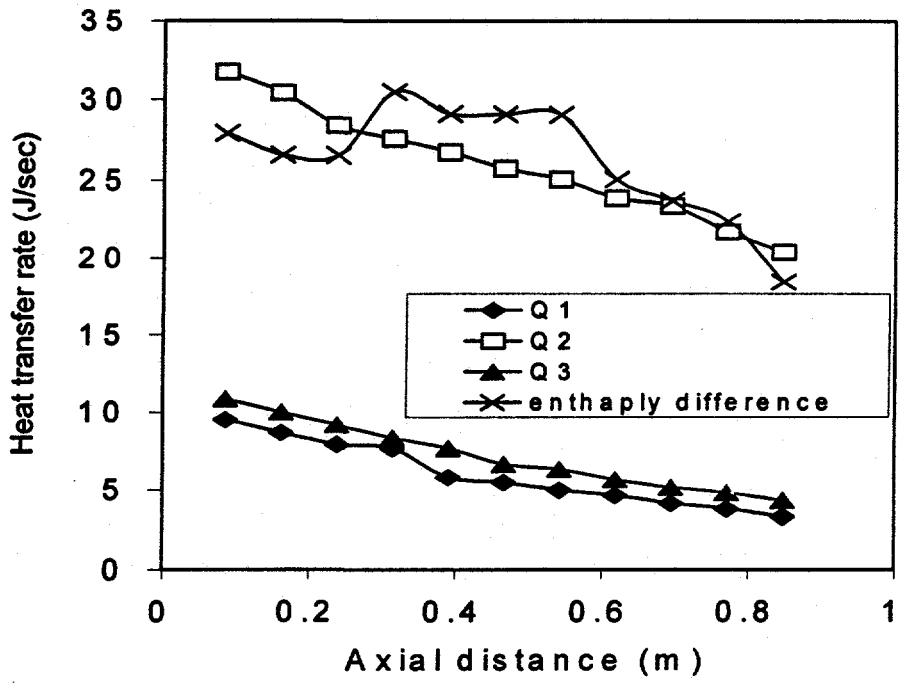

Figure 21 : Heat transfer rate distributions without pulsations in pipe submerged in a fluidized bed, Re=3200

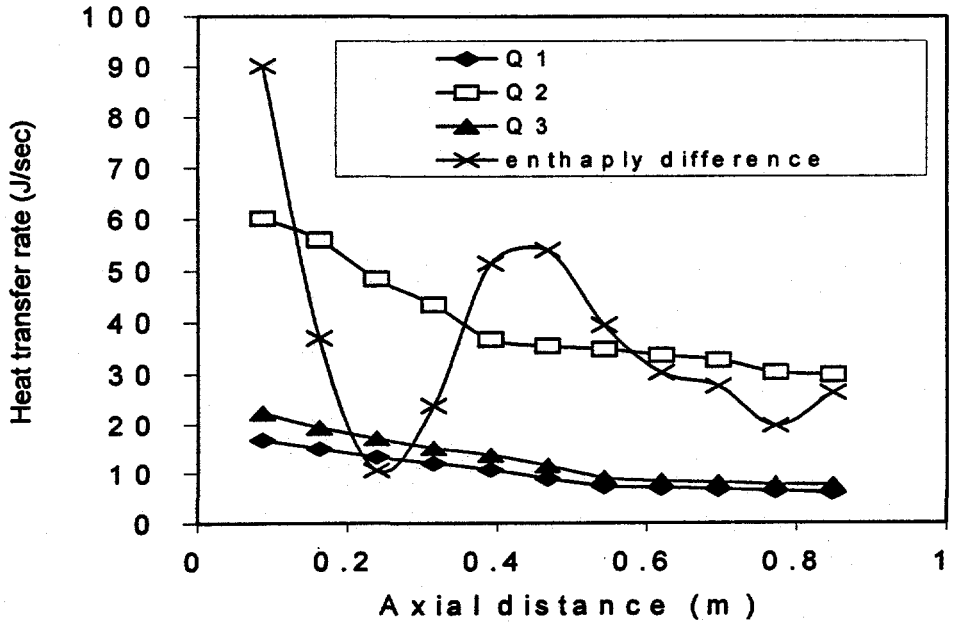

Figure 22 : Heat transfer rate distributions with pulsations in pipe submerged in a fluidized bed, Re=3200, f=389 Hz.

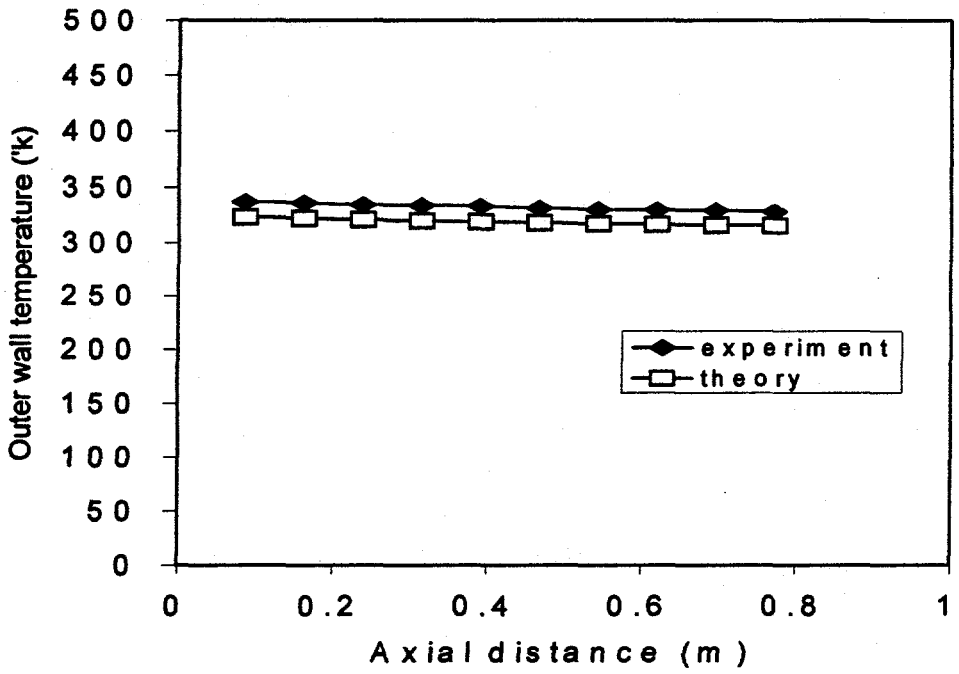

Figure 23: Outer wall temperature comparison between experiment and theory without pulsation in pipe submerged fluidized bed Re=3200, f=389 Hz.

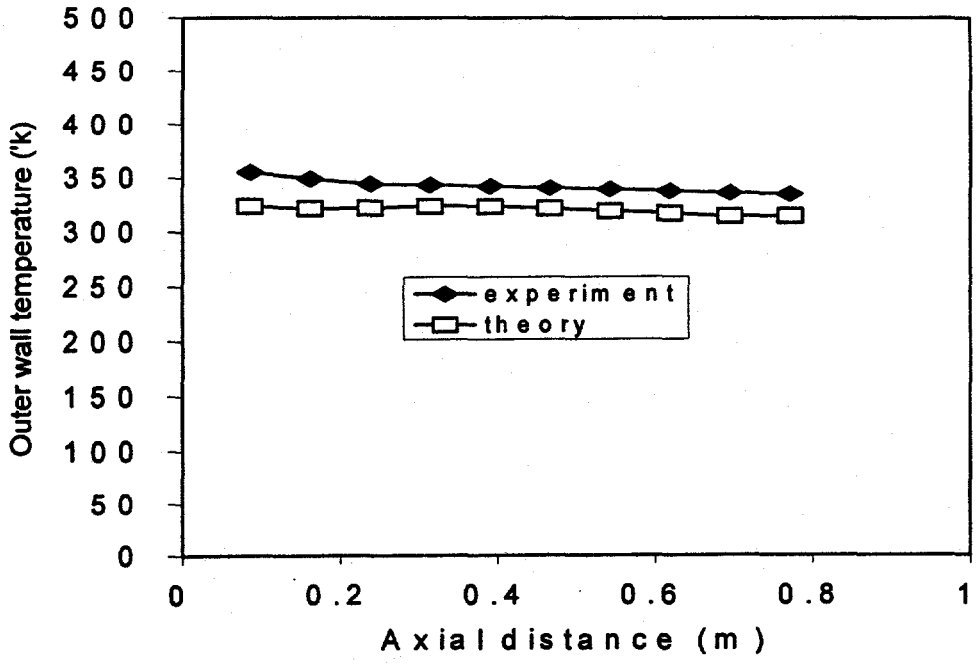

Figure 24: Outer wall temperature comparison between experiment and theory with pulsations in pipe submerged in a fluidized bed, Re=3200, f=389 Hz.

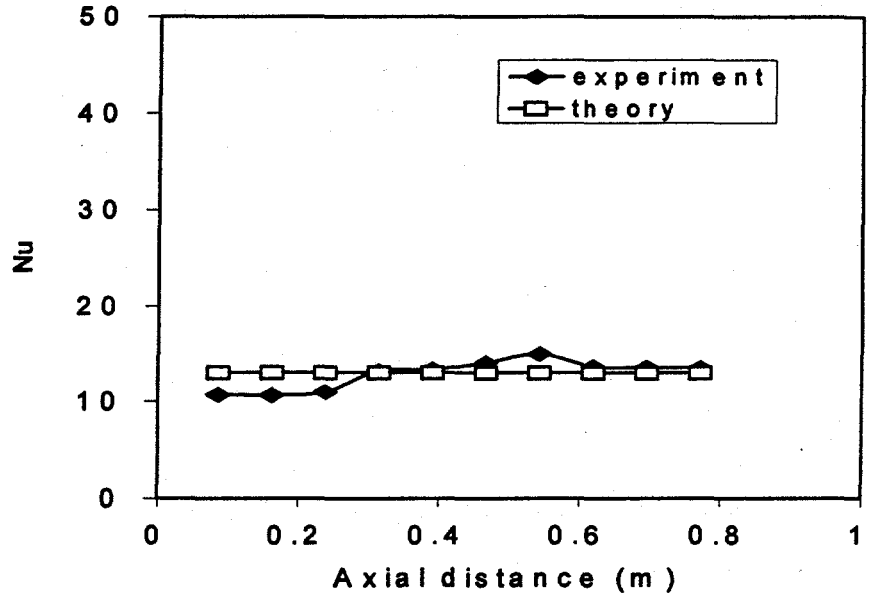

Figure 25: Nusselt number comparison between experiment and theory without pulsations in pipe submerged fluidized bed, re=3200, f=389 Hz.

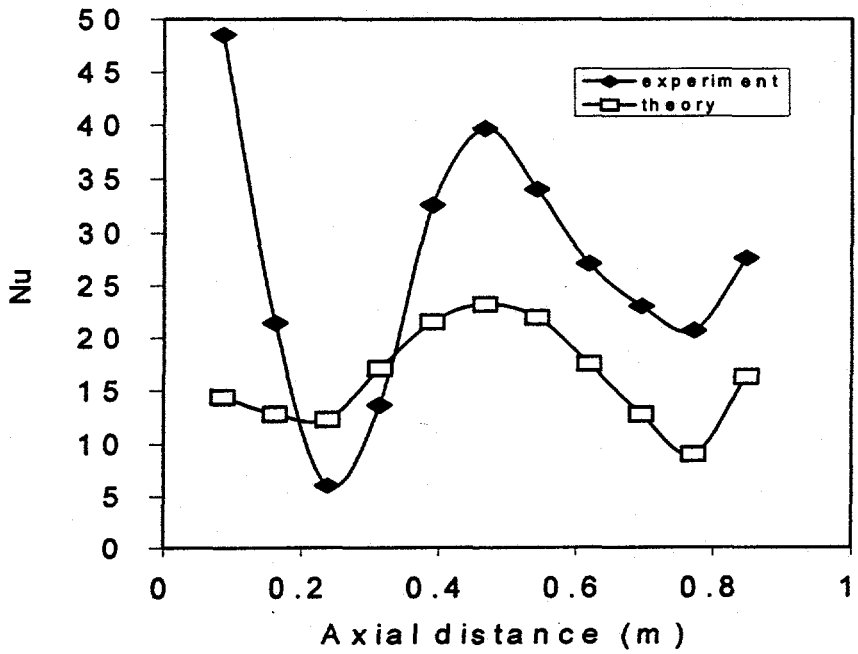

Figure 26: Nusselt number comparison between experiment and theory with pulsations in pipe submerged fluidized bed, re=3200, f=389 Hz.

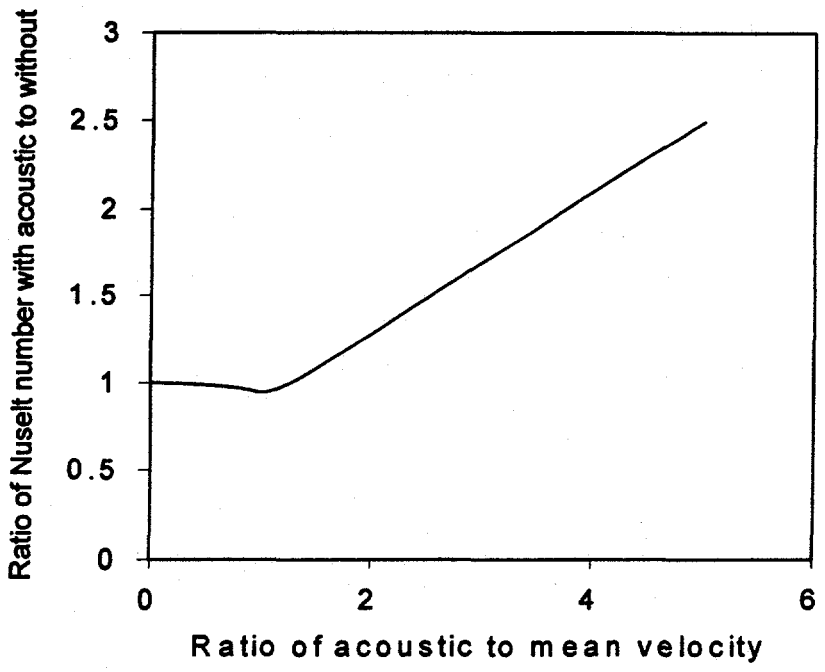

Figure 27: Theoretically determined Nusselt number ratio variation

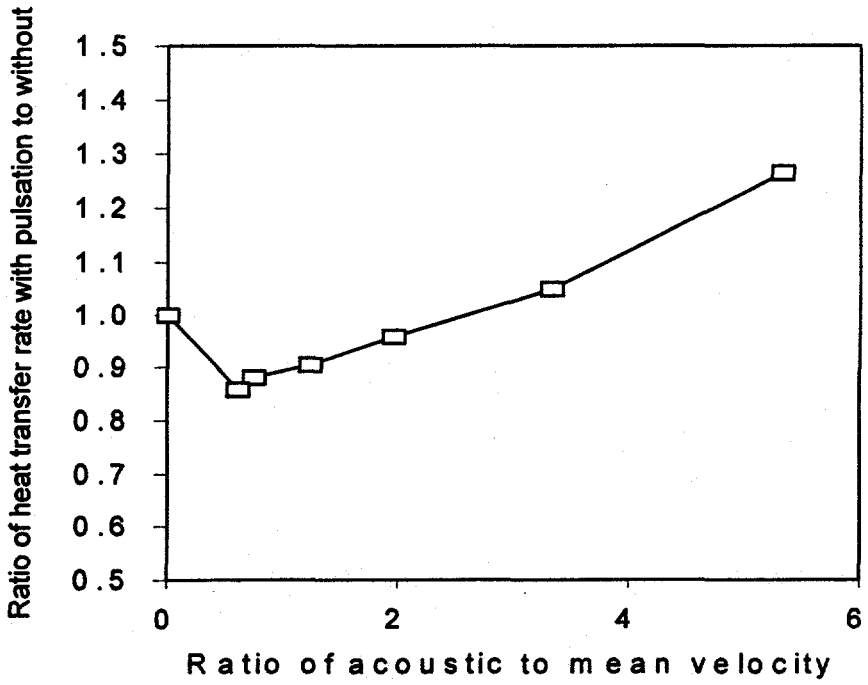

Figure 28: Experimentally determined heat transfer rate ratio variation f=389 Hz., SPL=167 dB.

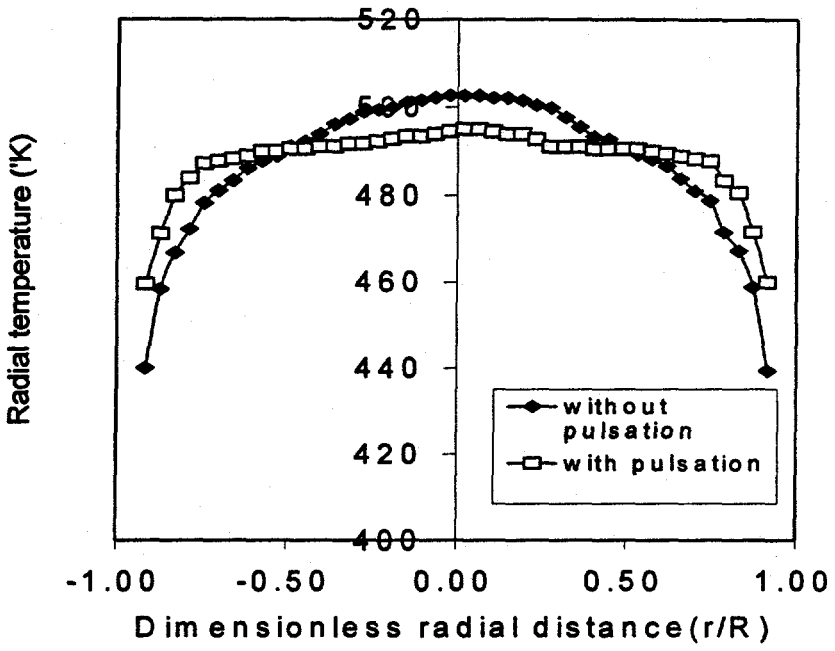

Figure 29: Comparison of radial temperature distributions without and with pulsations at low Reynolds number, Re=3200, f=389 Hz.

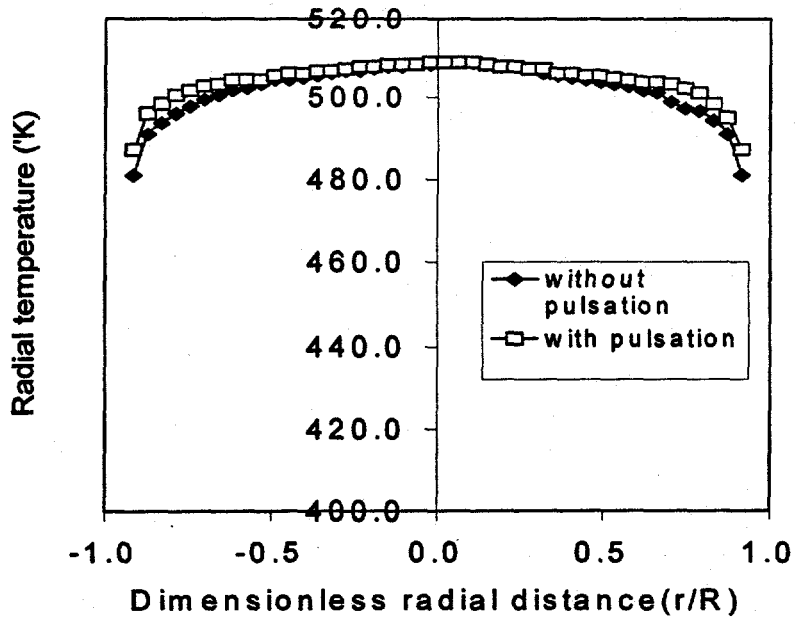

Figure 30: Comparison of radial temperature distributions without and with pulsations at high Reynolds number, Re=13400, f=404 Hz.

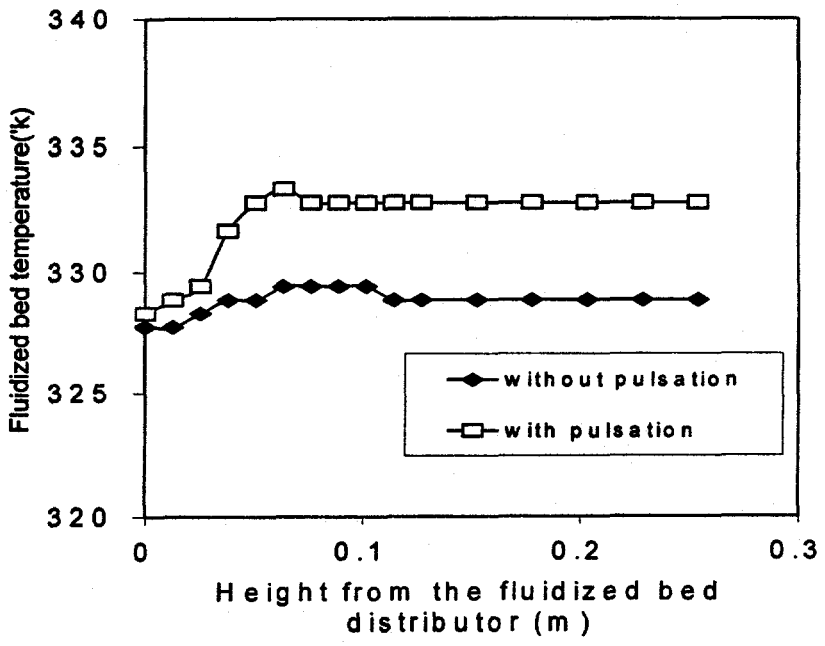

Figure 31: Vertical temperature distributions through the fluidized bed, Re=3200, f=389 hz. (Tail pipe located at 6 cm above distributor)

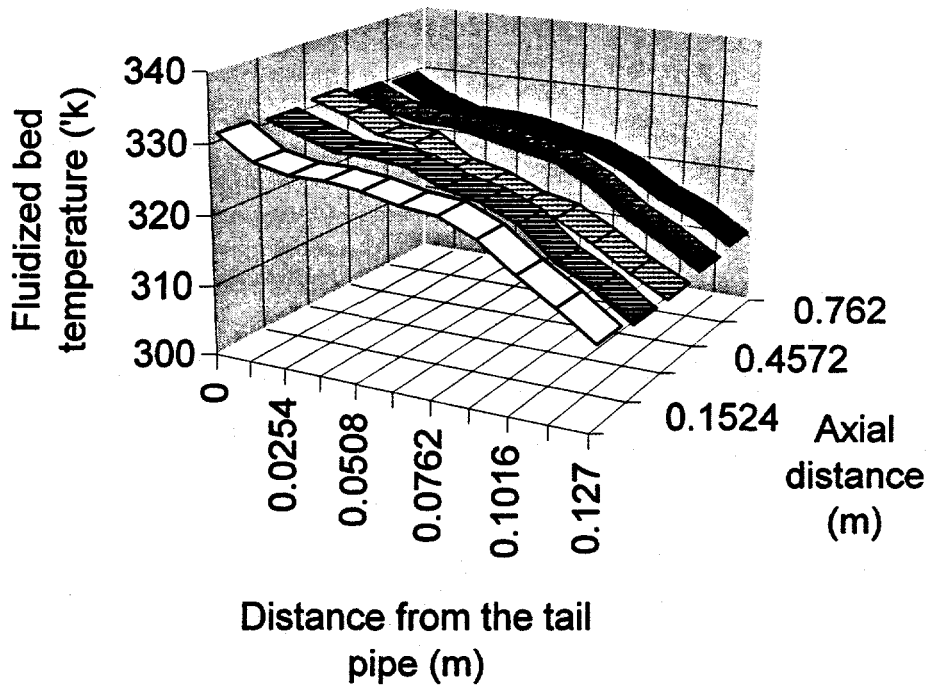

Figure 32: Lateral temperature distribution inside fluidized bed without pulsation in the pipe, f=389 Hz, Re=3200

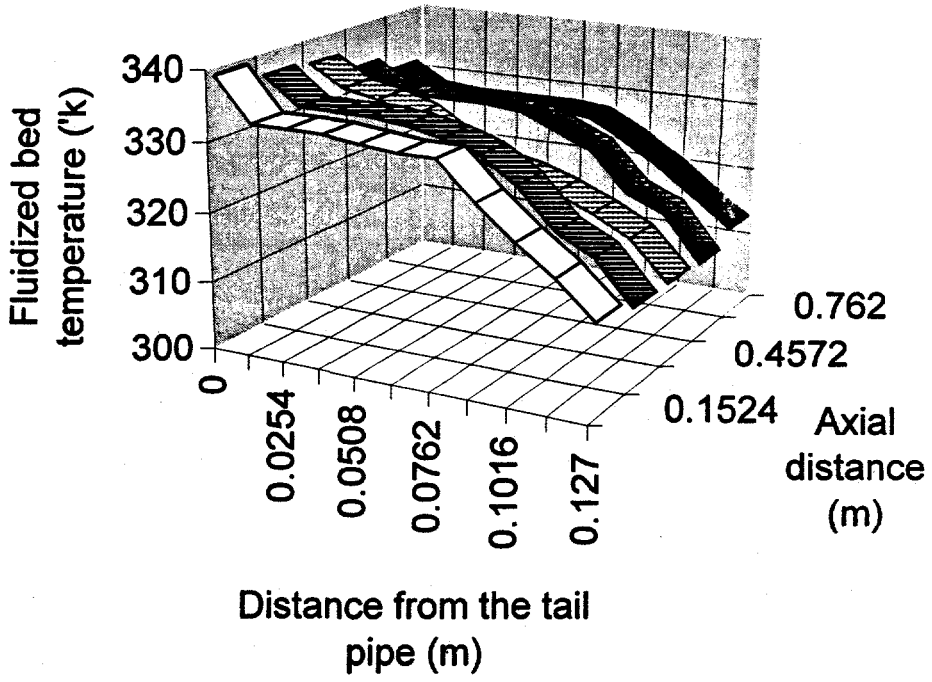

Figure 33: Lateral temperature distribution inside fluidized bed with pulsation in the pipe, f=389 Hz, Re=3200